JOURNAL OF PETROLOGY

Journal of Petrology, 2016, Vol. 57, No. 9, 1811–1832
doi: 10.1093/petrology/egw062
Original Article

OXFORD

A Calcium-in-Olivine Geohygrometer and its Application to Subduction Zone Magmatism

Maxim Gavrilenko[1,2], Claude Herzberg[1]*, Christopher Vidito[1], Michael J. Carr[1], Travis Tenner[3] and Alexey Ozerov[2]

[1]Department of Earth and Planetary Sciences, Rutgers University, Piscataway, NJ 08854, USA; [2]Institute of Volcanology and Seismology, Piip blvd, 9, 683006, Petropavlovsk-Kamchatsky, Russia; [3]Chemistry Division, Nuclear and Radiochemistry, Los Alamos National Laboratory, MSJ514, Los Alamos, NM 87545, USA

*Corresponding author. Telephone: (848) 445-3154. Fax: (732) 445-3374. E-mail: herzberg@rci.rutgers.edu

Received December 15, 2015; Accepted September 16, 2016

ABSTRACT

High-precision electron microprobe analyses were obtained on olivine grains from Klyuchevskoy, Shiveluch and Gorely volcanoes in the Kamchatka Arc; Irazú, Platanar and Barva volcanoes of the Central American Arc; and mid-ocean ridge basalt (MORB) from the Siqueiros Transform. Calcium contents of these subduction zone olivines are lower than those for olivines from modern MORB, Archean komatiite and Hawaii. A role for magmatic H_2O is likely for subduction zone olivines, and we have explored the suggestion of earlier workers that it has affected the partitioning of CaO between olivine and silicate melt. We provide a provisional calibration of $D_{CaO}^{Ol/L}$ as a function of magmatic MgO and H_2O, based on nominally anhydrous experiments and minimally degassed H_2O contents of olivine-hosted melt inclusions. Application of our geohygrometer typically yields 3–4 wt % magmatic H_2O at the Kamchatka and Central American arcs for olivines having ~1000 ppm Ca, which agrees with H_2O maxima from melt inclusion studies; Cerro Negro and Shiveluch volcanoes are exceptions, with about 6% H_2O. High-precision electron microprobe analyses with 10–20 μm spatial resolution on some olivine grains from Klyuchevskoy and Shiveluch show a decrease in Ca content from the core centers to the rim contacts, and a sharp increase in Ca in olivine rims. We suggest that the zoning of Ca in olivine from subduction zone lavas may provide the first petrological record of temporal changes that occur during hydration of the mantle wedge and dehydration during ascent, and we predict olivine H_2O contents that can be tested by secondary ionization mass spectrometry analysis.

Key words: olivine; calcium; subduction zone; magmatic water

INTRODUCTION

The introduction of water from a subducting lithospheric plate triggers melting in the mantle wedge above by lowering its solidus temperature (Fyfe & McBirney, 1975; Gill, 1981; Stolper & Newman, 1994; Grove *et al.*, 2006). Dehydration metamorphism and/or partial melting of the descending slab (Defant & Drummond, 1990) can introduce water in the form of a hydrous fluid, melt or a supercritical liquid (Manning, 2004; Kessel *et al.*, 2005). The most direct evidence for a role of elevated water in subduction zone magmatism comes from Fourier transform infra-red (FTIR) and secondary ionization mass spectrometry (SIMS) measurements of melt inclusions trapped and hosted by olivine (e.g. Wallace, 2005; Portnyagin *et al.*, 2007*b*; Kelley *et al.*, 2010; Mironov & Portnyagin, 2011). However, water is exsolved during ascent, indicating that these measurements must provide minimum bounds on the water contents of the primary magmas. Plank *et al.* (2013) summarized the existing database and concluded that the maximum H_2O content in melt inclusions from a single volcano or cinder cone is typically about 4%, and that this is characteristic of many volcanic arcs. However, those researchers also noted that some melt inclusions contain >6% H_2O (e.g. Auer *et al.*, 2009; Zimmer *et al.*, 2010), and examined a model wherein these high water contents could be degassed in

the crust, yielding ~4%. Additionally, diffusive loss of H^+ from melt inclusions to host olivine is rapid, indicating that measured H_2O contents may not be representative of the melt at the time of entrapment (Portnyagin *et al.*, 2008; Gaetani *et al.*, 2012; Bucholz *et al.*, 2013; Lloyd *et al.*, 2013; Le Voyer *et al.*, 2014). Uncertainty remains about the maximum water contents of undegassed primary magmas in subduction zone settings from melt inclusion studies.

As a potential complement to melt inclusion studies, we report progress using the partitioning of CaO between olivine and melt (i.e. $D_{CaO}^{Ol/L}$) as a proxy for magmatic H_2O content. The observation that $D_{CaO}^{Ol/L}$ is influenced by H_2O was originally made by Feig *et al.* (2006) from a comparison of experimental studies on wet and dry systems. We further explore the potential for olivine as a geohygrometer using several lines of evidence. First, we document reduction of olivine Ca contents from subduction zone volcanic rocks relative to those of mid-ocean ridge basalt (MORB), Hawaii, and Archean komatiites. We then compare olivine compositions and their H_2O-bearing melt inclusions with experimental data on the CaO contents of coexisting olivines and melts in nominally anhydrous systems; this provides a provisional calibration of our olivine geohygrometer. A critical evaluation is then made of experimental olivines synthesized in wet melting experiments, with special attention paid to the work of Tenner *et al.* (2012); it is shown that an improved geohygrometer is calibrated from olivine-hosted melt inclusions. We then evaluate magmatic H_2O contents by applying our geohygrometer to subduction zones, MORB, Hawaii, Gorgona, Ontong Java Plateau, and Archean komatiites. Special attention is paid to high-precision core–rim profiles of olivine grains from Klyuchevskoy and Shiveluch volcanoes in Kamchatka. We argue that such grains may be accidental crystals from the melting regime in the mantle wedge, and that they provide the first petrological record of temporal changes that occur during hydration of the mantle wedge and dehydration during ascent.

GEOLOGICAL BACKGROUND AND SAMPLES

Subduction zone olivine samples are from volcanoes located in the Kamchatka and Central American regions (Fig. 1). The Kamchatka Peninsula is an island arc with a complex geological history and structure. It has three distinct volcanic fronts—the Sredinny Range (which is now extinct), the Eastern volcanic front (EVF) and the Central Kamchatka depression (CKD). A junction with the Aleutian Arc (at ~56°N) complicates interpretation of the regional geodynamic setting [details have been provided in a review by Auer *et al.* (2009)]. However, the southern area (from ~53°N) of the Kamchatka Peninsula is considered to be a 'textbook case' of a subduction zone with a relatively rapid (over 80 mm a–1) near-normal convergence and a steep (over 50°) angle of subduction (Iwasaki *et al.*, 2013).

Klyuchevskoy and Shiveluch volcanoes belong to the CKD, which is characterized by unusual tectonic settings and exceptional volcanic productivity (Levin *et al.*, 2002; Portnyagin *et al.*, 2005, 2007*a*; Nikulin *et al.*, 2012). Klyuchevskoy is young (~6000 years), and produces frequent volcanic eruptions (Braitseva *et al.*, 1995) with an average annual magma output of ~0·045 km^3 (Melekescev, 1980; Braitseva *et al.*, 1995), making it one of the most productive volcanoes in the world. The Klyuchevskoy volcano has been the subject of many petrological and geochemical studies [see review by Mironov & Portnyagin (2011)]; it consists entirely of basalts and basaltic andesites (e.g. Ozerov, 2000; Almeev *et al.*, 2013), and it has been suggested that there is no crustal magma chamber below it (e.g. Ariskin *et al.*, 1995; Ozerov *et al.*, 1997). According to recent studies Klyuchevskoy is one of the few stratovolcanoes with little magma residence time

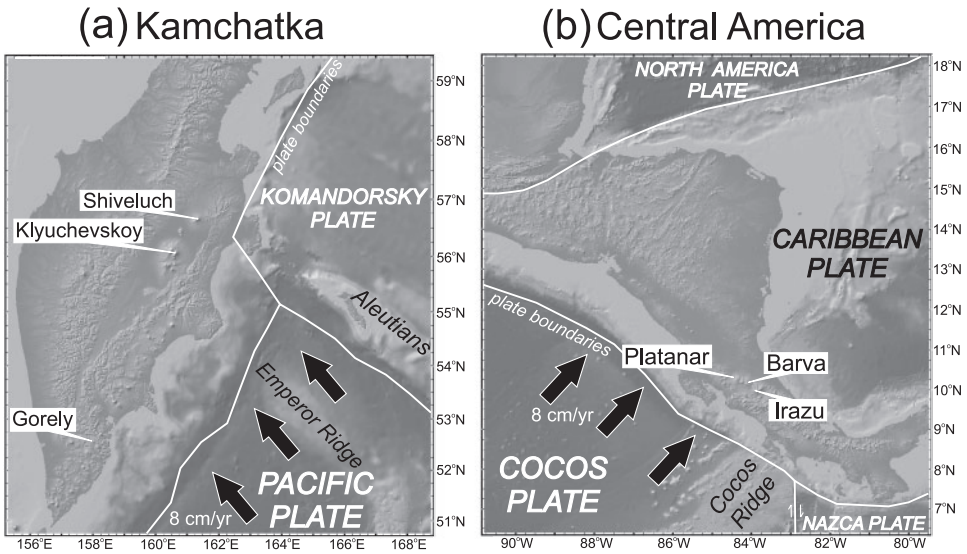

Fig. 1. Maps of sample locations. (a) Kamchatka Arc; (b) Central American Arc.

in the crust (e.g. Lees *et al.*, 2007; Ozerov, 2009; Mironov & Portnyagin, 2011; Kayzar *et al.*, 2014; Levin *et al.*, 2014). Thus, Klyuchevskoy volcano represents an end-member of magma source to surface transport, making it ideal to study the most primitive rocks produced in the mantle wedge. We analyzed olivines from Klyuchevskoy lava samples OK-03-07 (Bulochka flank eruption, ~3 ka) and OK-03-05 (Bilukai flank eruption, 1938). Corresponding whole-rock chemistries have been reported by Almeev *et al.* (2013) (as samples KL-5 and KL-40).

The Shiveluch andesitic volcano is located close to the junction of the Kamchatka and Aleutian arcs. It is active and large (~1000 km^3) and began erupting in the late Pleistocene (Ponomareva *et al.*, 2007; Gorbach *et al.*, 2013). Shiveluch erupts predominantly silicic magmas (andesites and dacites) with adakitic characteristics (e.g. Gorbach & Portnyagin, 2011); however, Shiveluch has had two episodes of mafic eruptions (3600 bp and 7600 bp), and resulting basalts are phlogopite- and amphibole-bearing (Volynets *et al.*, 1997). We analyzed olivine grains from Shiveluch basaltic tephra sample 00K15 (3600 BP mafic eruption); the complete description and whole-rock chemistry have been provided by Ponomareva *et al.* (2007).

The Gorely shield-shaped volcano is located within the south segment of EVF on the Kamchatka Peninsula. It is composed of basalts to rhyolites typical of island-arc compositions (e.g. Tolstykh *et al.*, 2012; Seligman *et al.*, 2014; Gavrilenko *et al.*, 2016). We interpret high-precision olivine analyses from Gorely lava samples reported by Gavrilenko *et al.* (2016).

All of the studied Central American olivine samples come from the Cordillera Volcanica Central (CVC) of Costa Rica. The volcanoes in this cordillera have enriched trace element and isotopic signatures; such signatures are similar to those from the Galapagos hotspot, as well as those from other ocean island basalts (Gazel *et al.*, 2009, 2011).

Irazú is the largest volcano in Costa Rica and marks the southeastern end of the volcanic front caused by subduction of the Cocos Plate. It started to erupt at ~600 ka, but sits on the deposits of older eruptions that began at ~2 Ma, a stratigraphy is common throughout the CVC. We analyzed olivine grains in Irazú sample CR-IZ-02-1 (Western Cervantes lava flow). Details of this sample have been given by Alvarado *et al.* (2006) and Carr *et al.* (2013).

The Barva volcano is slightly smaller than Irazú and has had no historical activity; thus, it is not well studied. It is hypothesized to completely share the petrological and geochemical characteristics of Irazú (Alvarado *et al.*, 2006). We analyzed olivine grains in Barva sample CR-B2 (Carr *et al.*, 2013).

Platanar is a smaller volcanic center relative to Barva and Irazú, and the volcanoes forming it are better defined. However, Platanar has a complicated history and lacks recent activity (Alvarado & Carr, 1993). We analyzed olivine grains from sample CR-PP8, which is one of the unusual alkaline shoshonitic basalts. The Platanar sample is from a cluster of cinder cones just behind the volcanic front called Aguas Zarca. Platanar volcano information, including details of its samples, has been provided by Alvarado & Carr (1993) and Carr *et al.* (2013).

As we are interested in understanding the role of magmatic H_2O in the calcium content of olivine, we need an anhydrous reference frame. Therefore, we have obtained both glass and high-precision olivine data on sample D-20-15 from the Siqueiros Transform of the East Pacific Rise (Perfit *et al.*, 1996; Hays, 2004). Measurements of olivine-hosted melt inclusions in Siqueiros samples show low H_2O contents (Saal *et al.*, 2002).

ANALYTICAL METHODS

Olivine analyses were conducted on a JEOL JXA-8200 electron microprobe at Rutgers University. Major element and trace element (Mn, Ni, Ca and Al) data were obtained using a slightly modified version of the high-precision method of Sobolev *et al.* (2007). A beam current of 300 nA and an accelerating voltage of 20 kV were used for all analyses of natural olivines. We also examined experimental evidence for H_2O in olivine chemistry and, for such olivines, we employed a reduced accelerating voltage of 15 kV, combined with a 300 nA beam current, owing to their small size. For all high-precision work, count times on the elements are as follows: 50 s for Si, 50–80 s for Mg, 100 s for Fe, 150–250 s for Ni, 150–500 s for Mn, 150–600 s for Ca and 500 s for Al. We calibrated on synthetic fayalite or tephroite for Si, synthetic forsterite for Mg, synthetic fayalite for Fe, synthetic tephroite for Mn, synthetic Ni_2SiO_4 for Ni, Kakanui augite (USNM 122142) or chromian augite (NMNH 164905) for Ca, and Kakanui pyrope (USNM 143968) for Al. We used a San Carlos olivine standard only for drift correction, and it was analyzed at regular intervals throughout every run session. Detection limits at 3σ (99% confidence level) and errors (2σ) were obtained from the Probe for Windows program (Donovan, 2012). Average detection limits for Si, Mg and Fe are 31 ppm, 44 ppm and 36 ppm, respectively. Average detection limits for trace elements Ni, Mn, Ca and Al are 21 ppm, 19 ppm, 10 ppm and 13 ppm, respectively. The average relative 2σ errors of Si, Mg and Fe are ~0·10%, ~0·13% and ~0·29% respectively. Average 2σ errors for trace elements Ni, Mn, Ca and Al are 33 ppm, 30 ppm, 17 ppm and 23 ppm respectively. Two standard deviations of Ni, Mn, Ca, Al and Mg-number for the San Carlos olivine analyses ($n = 659$) in our study are 32 ppm, 25 ppm, 16 ppm, 20 ppm and 0·1% units, respectively. In most cases oxide totals were within ±1% of 100%. Chemical formulae were calculated for all analyses, and we accepted only data with T-sites having 1·01–0·99 cations and M-sites having 2·02–1·98 cations when normalized to four oxygens.

Natural olivine data, as well as details of the analytical conditions, are given in Supplementary Data Table

A1 (all Supplementary Data are available for downloading at http://www.petrology.oxfordjournals.org). We obtained detailed core–rim analyses at 10–20 μm intervals on some olivine grains, and scanning electron microscope (SEM) images are also provided. As discussed below, we also reanalyzed the experimental olivines of KLB-1 from Tenner *et al.* (2012), and these are given in Supplementary Data Table A2. Kamchatka data were obtained on olivine grain mount separates, which decreases the possibility of secondary Ca fluorescence from glass. Olivines from Siqueiros MORB and Central America were analysed in thin section, and data collection was restricted to their cores. Olivines in the experiments of Tenner *et al.* (2012) were embedded in quench glass, and data were obtained away from rims to reduce the risk of secondary Ca fluorescence.

Glass analyses for Siqueiros MORB sample D-20-15 were conducted on the JEOL JXA-8200 electron microprobe at Rutgers University. Glass compositions were measured using a current of 10 nA, an accelerating voltage 15 kV, and a 16 μm raster mode. On-peak count times were: 5 s for Na; 20 s for K and P; 30 s for Si and Al; 50 s for Mg, Ca, Ti and Cr; 100 s for Fe; 90 s for Ni; and 150 s for Mn. A time-dependent intensity (TDI) correction was applied to Na and K. Glass data are given in the Supplementary Data Table A4.

CALCIUM CONTENTS OF OLIVINE

Primitive olivine phenocrysts from Siqueiros MORB have Mg-numbers of 91·0 and contain 2000 ppm Ca (Fig. 2a; Supplementary Data Table A1); new data reported here are in good agreement with those of Sobolev *et al.* (2007). Barberton olivines of the Komati Formation (Herzberg *et al.*, 2013) have slightly lower Ca contents and higher Mg-numbers than MORB olivines. These primitive MORB and Barberton olivines are also similar to computed olivines from anhydrous primary magmas of a peridotite source that formed by accumulated fractional melting (Herzberg, 2011; Herzberg *et al.*, 2013), providing evidence that they crystallized from melts with little H_2O.

Representative olivines having much lower Ca contents than MORB and Barberton olivines are plotted in Fig. 2a. Almost all olivines from the shield-building volcanoes on Hawaii are examples, but only those from Mauna Loa are plotted to preserve clarity (Sobolev *et al.*, 2007). It has been inferred that Hawaiian olivines are lower in Ca than MORB and Barberton because they crystallized from parental magmas that are low in CaO, when normalized to constant MgO, owing to CaO retention in a pyroxenite source (Herzberg, 2006, 2011).

Ca contents of olivines from subduction zone volcanoes are lower than those from Hawaii. Olivines from Klyuchevskoy and Shiveluch (Fig. 2a) have the highest Mg-numbers and lowest Ca contents. Similar to Hawaii, it may be inferred that such olivines crystallized from melts of a pyroxenite source. However, this explanation is unlikely because, as shown below, the Ni contents of olivines from Klyuchevskoy and Shiveluch are low and are more consistent with a peridotite source. Olivines from Gorely, Irazú, Platanar, and Barva have about 1000 ppm Ca at the highest Mg-numbers (Fig. 2a and b), similar to some olivines from Klyuchevskoy; olivines from Shiveluch have the lowest Ca contents in this study.

The effect of temperature on olivine Ca content is insignificant (Feig *et al.*, 2006), which is confirmed by reported maximum crystallization temperatures based on the Al-in-olivine thermometer for MORB, large igneous provinces (LIPs) (Coogan *et al.*, 2014), and arcs (Mironov *et al.*, 2015; Gavrilenko *et al.*, 2016). MORB and LIP olivines have similar Ca contents (~2000 ppm), but LIP crystallization temperatures are much higher than for MORB (Herzberg *et al.*, 2007; Herzberg & Gazel, 2009; Coogan *et al.*, 2014). However, many arc olivines have low Ca contents (~1000 ppm) and crystallize at similar temperatures to MORB olivines.

It is not plausible that the low-Ca subduction zone olivines originated as xenocrysts from the lithosphere. Ionov (2010) reported data from peridotite xenoliths from the Avacha volcano in southern Kamchatka, and they contain olivine with 276 ± 233 ppm Ca, much lower than for subduction zone olivines. Although we cannot properly evaluate the quality of olivine data in open access databases, the Ca content of olivine in garnet lherzolite xenoliths averages 427 ± 249 (1σ) ppm for 331 samples, and the Ca content of olivine in spinel lherzolite xenoliths averages 508 ± 385 ppm (1σ) for 1020 samples (http://georoc.mpch-mainz.gwdg.de/georoc/). Kamenetsky *et al.* (2006) also reported olivines from Solomon Islands picrites, which are similar to Klyuchevskoy olivines in that they have low Ca and high Mg-numbers, and reviewed the evidence that such olivines could not be lithosphere xenocrysts; this included trapped melt and mineral inclusions, nonanhedral shapes, and chemical zoning, which point to a magmatic origin.

Kamenetsky *et al.* (2006) concluded that subduction olivine Ca contents are low because they crystallized from low-Ca magmas. However, the relationship between parental magma Ca content and the Ca content of its crystallizing olivines is complex. Many Hawaiian magmas have CaO contents that are comparable with those of subduction zone lavas, yet their olivines have higher CaO contents (Fig. 2). Parental magma compositions in equilibrium with reported high-precision olivines from MORB, Hawaii, Archean komatiites, and subduction zones are calculated using the methods discussed in the Supplementary Data, and results are given in Supplementary Data Table A3. Results in Fig. 3 show that the CaO contents of olivine can vary by a factor of three for parental magmas having 7–10% CaO. In most cases, the partition coefficient of CaO between olivine and melt is dominated by olivine. Below, we examine evidence that extreme Ca depletions in subduction zone olivines are the result of elevated magmatic H_2O.

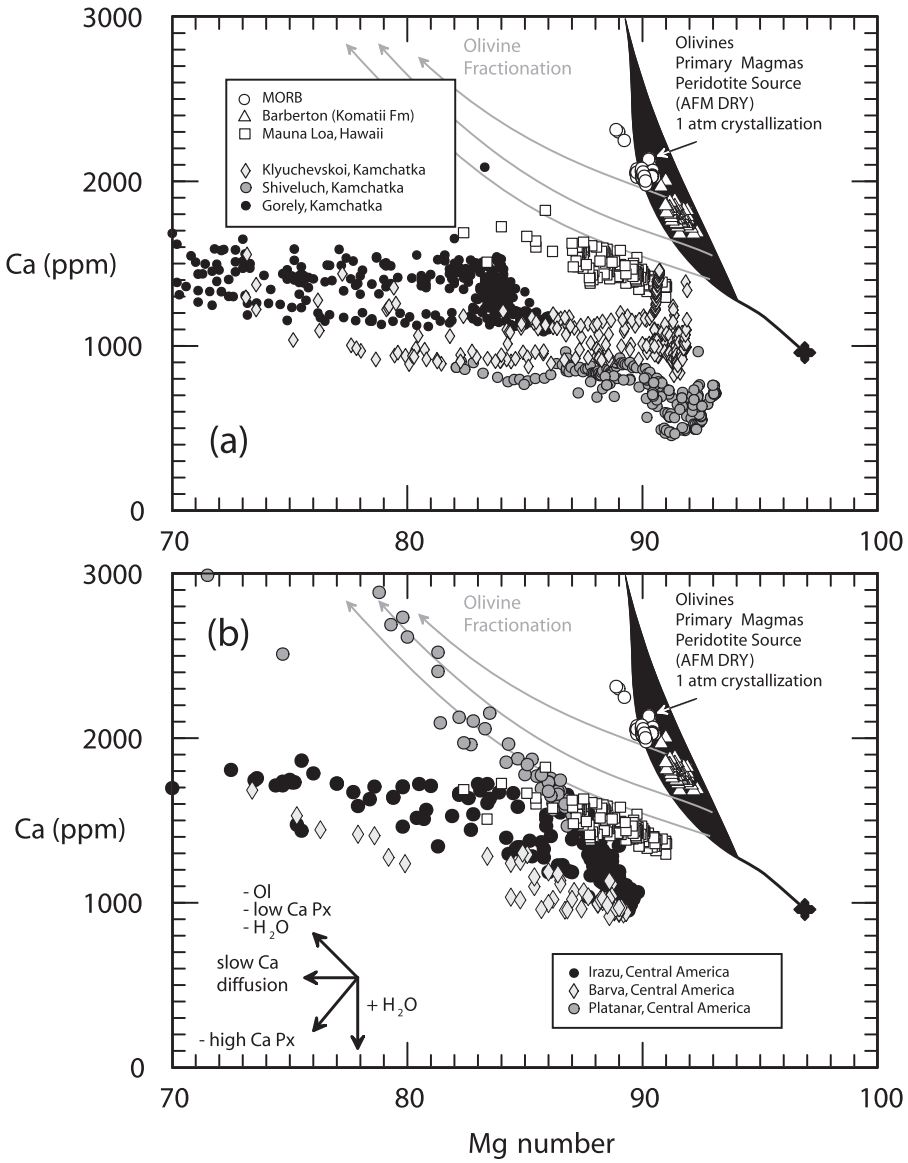

Fig. 2. Mg-numbers and Ca contents of measured and model olivines [Mg-number = molar 100MgO/(MgO + FeO)]. Black fields represent model olivines that would crystallize at the surface from primary magmas of anhydrous peridotite, formed by accumulated fractional melting (Herzberg, 2011; Herzberg *et al.*, 2013); black cross terminations are olivine compositions for total melting of anhydrous peridotite. Symbols are olivines that have been measured by a high-precision electron analytical protocol. Olivines from Siqueiros MORB are high-precision measurements on sample D-20-15 in the present study. Barberton olivines were reported by Herzberg *et al.* (2013). Olivines for Mauna Loa are samples SR0018-0.10 and SR0098-2.00 from Sobolev *et al.* (2007). (a) Olivines from the Kamchatka Arc; (b) olivines from the Central American Arc. For the three Central American volcanoes, primitive olivines have ~1000 ppm Ca at Mg-numbers of 89–90. For all subduction olivines, the arrows in (b) illustrate approximate compositional vectors expected from olivine or low-Ca pyroxene fractionation, Ca-clinopyroxene fractionation, magmatic H_2O dehydration, magmatic H_2O entry and slow Ca diffusion.

Zoning in olivines from Kamchatka

High-precision electron microprobe traverses were obtained at 10–20 μm intervals from cores to rims of several olivine grains within a lava flow (sample OK-03-07, Bulochka flank eruption) from the Klyuchevskoy volcano (Fig. 4). Cores and rims are separated by chemical boundaries that are sharp and well-defined in some cases. For example, Mg-number is high and constant within the cores, but decreases within the rims. In addition, the Ni contents of olivine cores are almost constant, dropping sharply in the rims. Diffusion has clearly played a role in Klyuchevskoy olivine zoning. For example, in olivine grain 13 the Mg-number is ~91·8 from the center of the grain to 390 μm, then it decreases sharply to 73·6 at the rim edge (Fig. 4a). In contrast, corresponding increases in Ca concentration and decreases in Ni concentration occur at 480 μm and 450 μm relative to the center of the grain (Fig. 4b and 4c, respectively). Radial chemical offsets also occur in olivine grain 26. Such core–rim offsets are difficult to comprehend if the olivines had grown as phenocrysts from a melt. In the sections that follow, we provide evidence

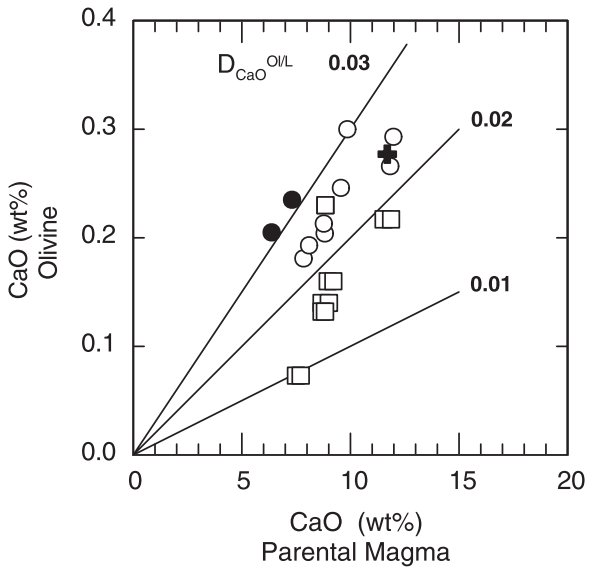

Fig. 3. CaO contents of olivines and their parental magmas (Supplementary Data Table A3). Black cross, MORB; filled circles, Archean komatiites; open circles, Phanerozoic plumes (Hawaii, Gorgona, Ontong Java Plateau); open squares, subduction zones (Kamchatka, Central America).

that these were exotic grains, which were plucked from the melting region, and that the rims of such grains record diffusion profiles that formed by partial re-equilibration with their host magmas during ascent in the volcano conduit. The rim profiles predict diffusion coefficients increasing in the manner Ca $<$ Ni $\leq$ Mn $=$ Fe–Mg, which are consistent with experimental studies (Coogan *et al.*, 2005; Chakraborty, 2010). Remarkably, the diffusion profiles and their core–rim offsets are very similar to those reported by Qian *et al.* (2010) for a natural olivine xenocryst that was immersed in a dioritic magma. We note, however, that core–rim boundaries are equidistant for grain 21, indicating minor partial re-equilibration with melt in this case.

Olivine grains from Shiveluch volcano (sample 00K15, basaltic tephra from 3600 bp eruption) display some similarities, but also some differences in their core–rim profiles (Fig. 5), when compared with those from Klyuchevskoy (Fig. 4). An important similarity is a nearly constant Mg-number and Ni concentration up to 500 μm from the center of the grains. However, Shiveluch core Ni concentrations are restricted to values ranging from 3000 to 3100 ppm, which agree with

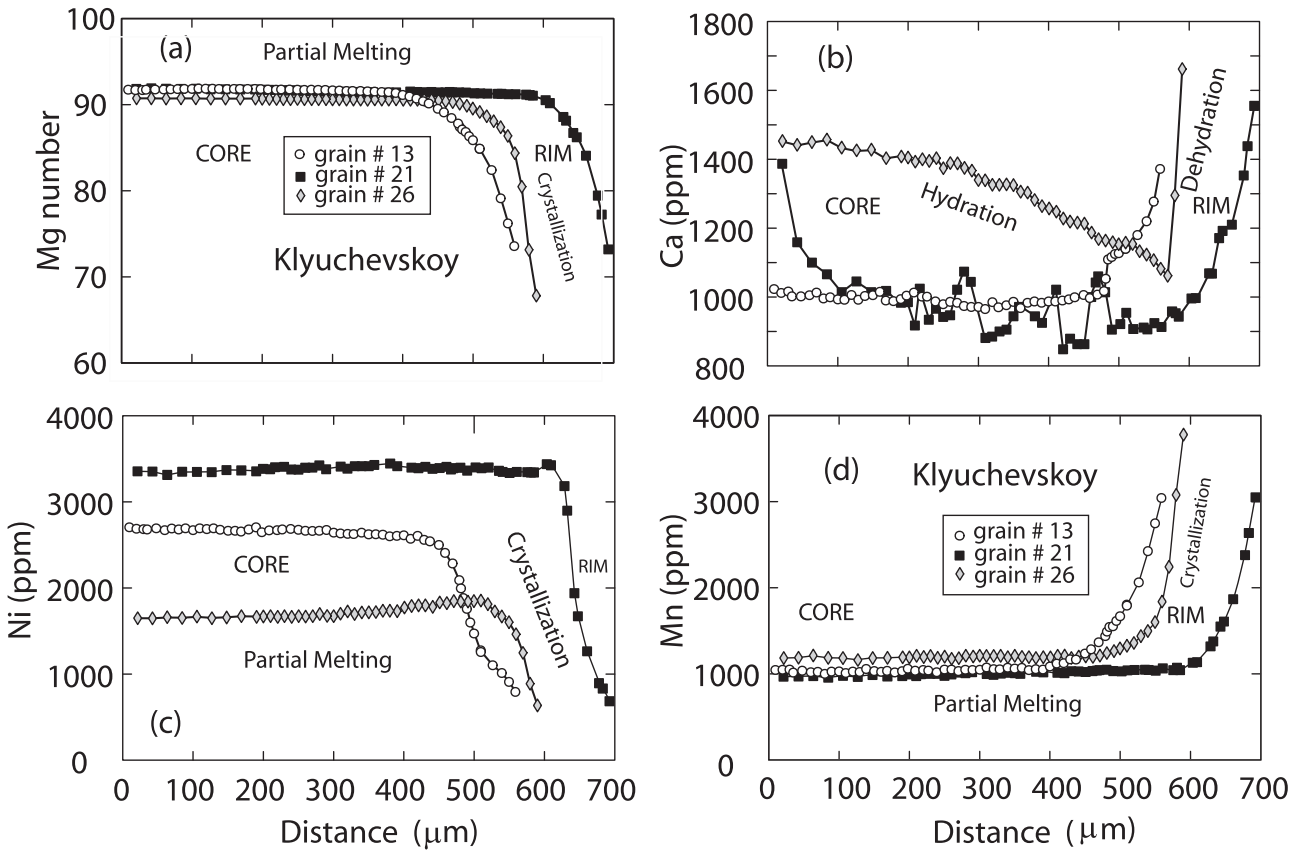

Fig. 4. High-precision EMPA core–rim profiles for three olivine grains from the Klyuchevskoy volcano. Small core–rim variations in Mg-number, Ni, and Mn are a result of partial melting; large intergrain variations in Ni are interpreted as resulting from variable addition and subtraction of sulfide or some other phase. The substantial decrease in Ca for grain 26 is interpreted as resulting from H_2O addition from the slab; the increase in Ca in the rim reflects partial crystallization of olivine and dehydration. Partial crystallization of olivine is responsible, based on the decrease in rim Mg-number and Ni content, and increase in Mn content. The slight reversed zoning in grain 26, where Ni increases in the outer core at around 500 μm, should be noted.

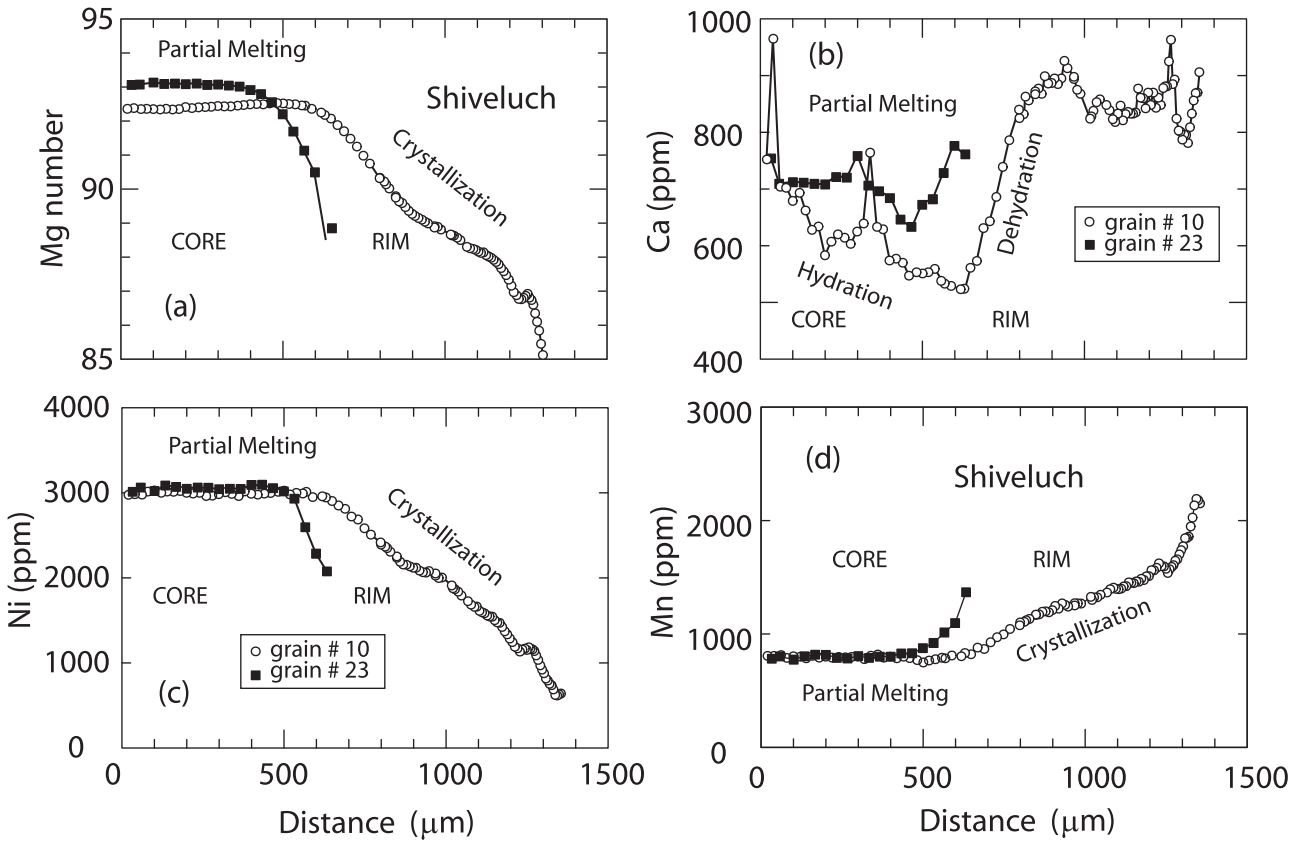

Fig. 5. High-precision EMPA core–rim profiles for two olivine grains from the Shiveluch volcano. Partial melting, crystallization, hydration and dehydration processes are suspected to influence core–rim zoning, similar to results shown in Fig. 4.

computed olivine grains from peridotite partial melts (Herzberg, 2011; Herzberg *et al.*, 2013). For comparison, olivine cores from Klyuchevskoy have nearly constant Ni contents, but there are large intergrain differences: ~3300 ppm for grain 21, 2700 ppm for grain 13, and 1600 ppm for grain 26 (Fig. 4c). Many primitive MORB olivines show Ni depletion, which has been interpreted to be the result of Ni scavenging by sulfide retention in the melting regime (Herzberg, 2011). Klyuchevskoy olivine Ni variations are larger than those for MORB, indicating perhaps Ni extraction by sulfides or some other phase (Li *et al.*, 2013) in subduction environments. Alternatively, we suggest below that this variation in Ni may be a response to melt–rock reaction in the mantle.

For Klyuchevskoy, there is a gradual but substantial decrease in Ca in olivine grain 26 from 1450 ppm at the center to 1060 ppm at the rim contact (Fig. 4b). Primitive olivines having ~1000 ppm Ca are also commonly observed in Central America (Fig. 2b). Below we provide evidence that Ca zoning in Klyuchevskoy olivine is suggestive of time-dependent H_2O addition as indicated in Fig. 4b. Similar core-to-rim drops in Ca were also reported by Kamenetsky *et al.* (2006) for olivines from Solomon Islands picrites. In contrast to cores, Klyuchevskoy olivine rims record an increase in Ca concentrations, as most vividly illustrated within grain 26 (Fig. 4b). This is not an artifact of secondary Ca fluorescence from glass because the olivines are grain mounts. Shiveluch olivine grain 10 is similar to Klyuchevskoy olivine in that it exhibits a drop in Ca from the core center to the core–rim contact, then an increase in Ca to the grain edge (Fig. 5b).

CALCIUM ZONING IN OLIVINE: A STRATEGY FOR ITS EVALUATION

For basaltic melts, there must always be an increase in Ca content along a liquid line of descent (LLD) during fractional crystallization of Ca-poor phases such as olivine and low-Ca pyroxene; olivine phenocrysts that grow along such an LLD must also exhibit an increase in Ca content, and they should exhibit Ca contents that increase from core to rim. This prediction is at odds with the measured gradual drop in Ca within some olivine cores at a constant Mg-number (Figs 4 and 5). We now explore the possibility that Ca zoning in olivine is influenced by magmatic H_2O. This was motivated by experimental observations described below, and the suggestion made by Feig *et al.* (2006) that H_2O will affect the partitioning of calcium between olivine and melt:

$$D_{CaO}^{Ol/L} = CaO_{Olivine}/CaO_{Liquid} \quad (1)$$

where $D_{CaO}^{Ol/L}$ is the distribution (or partition) coefficient, and CaO refers to the weight per cent CaO in olivine and liquid.

Ideally, what is needed is a model of $D_{CaO}^{Ol/L}$ in anhydrous systems, and how it is affected by H_2O. There are many models of $D_{CaO}^{Ol/L}$ for anhydrous melts (Watson, 1979; Ford *et al.*, 1983; Jurewicz & Watson, 1988; Beattie *et al.*, 1991; Libourel, 1999; Mysen, 2007, 2008; Tuff & O'Neill, 2010). However, the problem with working with zoned olivines is that the Ca contents are known (Figs 4 and 5), but we do not know the Ca contents of the melts from which they grew. This incomplete information places a limit on any comprehensive model no matter how accurate it may be. The strategy that we adopt is to start with a simple model of $D_{CaO}^{Ol/L}$ in nominally anhydrous systems, examine how it is affected by H_2O, estimate parental magma CaO contents, and make predictions about olivine H_2O content that can be tested with SIMS analysis.

PARTITIONING OF CaO BETWEEN OLIVINE AND SILICATE LIQUID

Feig *et al.* (2006) presented a preliminary parameterization of $D_{CaO}^{Ol/L}$ as a function of olivine Mg-number, and showed from experimental data that it decreased with increasing H_2O. A difficulty with this approach is that olivine with an Mg-number of 90, for example, can be in equilibrium with melts over a wide range of temperatures (Herzberg *et al.*, 2007), and that temperature may affect $D_{CaO}^{Ol/L}$. However, the MgO content of a melt in equilibrium with olivine is positively correlated with temperature (e.g. Herzberg & Asimow, 2015). Therefore, we examine $D_{CaO}^{Ol/L}$ as a function of melt MgO content, and evaluate whether such a comparison sufficiently captures the full range of variables that affect it.

A parameterization of $D_{CaO}^{Ol/L}$ and MgO for anhydrous systems provides the necessary reference frame for examining the effects of H_2O. Figure 6a illustrates results of nominally anhydrous experimental studies, with compositions ranging from fertile peridotite to basalt, and at temperatures of 1150–2050 °C, pressures of 1 atm to 14·4 GPa, and for melt fractions from near-zero to 0·86 (for peridotite) (Takahashi & Kushiro, 1983; Canil, 1992; Grove *et al.*, 1992; Kinzler & Grove, 1992; Baker & Stolper, 1994; Toplis & Carroll, 1995; Herzberg & Zhang, 1996; Yang *et al.*, 1996; Kinzler, 1997; Parman *et al.*, 1997; Gaetani & Grove, 1998; Robinson *et al.*, 1998; Taura *et al.*, 1998; Walter, 1998; Falloon *et al.*, 1999, 2008; Falloon & Danyushevsky, 2000; Laporte *et al.*, 2004; Parman & Grove, 2004; Sano & Yamashita, 2004; Mibe *et al.*, 2006; Wang & Gaetani, 2008; Chalot-Prat *et al.*, 2010, 2013; Longhi *et al.*, 2010; Davis *et al.*, 2011; Le Roux *et al.*, 2011; Matzen *et al.*, 2011, 2013; Till *et al.*, 2012). There are broadly two populations of experimental data, and uncertainties in their description were minimized by separating them at 13% MgO (Fig. 6a). Linear regressions of the two populations result in two segments intersecting at 11·1% MgO. For the low-MgO population (i.e. MgO $<$ 11·1%)

$$D_{CaO}^{Ol/L} = -0{\cdot}0043\mathrm{MgO} + 0{\cdot}072 \quad (2)$$

(1 RMSE $= \pm 0{\cdot}007$). For the high-MgO population (i.e. MgO $>$ 11·1%)

$$D_{CaO}^{Ol/L} = 0 \cdot 00042\mathrm{MgO} + 0 \cdot 0196 \quad (3)$$

(1 RMSE $= \pm 0{\cdot}004$). The experimental data are described to within $\pm 0{\cdot}007$ for the low-MgO population and $\pm 0{\cdot}004$ for the high-MgO population. These equations are perfectly valid within the stated uncertainty bounds, but we acknowledge that other parameterizations may do a better job of minimizing the uncertainties.

The thermodynamic basis for the two segments has not been examined in detail. However, we expect that the low-MgO population probably involves greater participation of clinopyroxene, and that melt CaO contents can be driven down over relatively small ranges of temperature and melt fraction. Uncertainties in the regressions are large, and cannot be reduced by consideration of an independently adjustable olivine liquidus temperature term, which is captured by the MgO contents of the melts (Herzberg & Asimow, 2015). In addition, it is unlikely that the parameterization can be improved by an independently adjustable pressure term; for instance, 3–7 GPa experimental results of Walter (1998) reveal that increases in pressure are related to increases in olivine liquidus temperatures, which are captured by MgO content. As might be expected, most of the uncertainty in $D_{CaO}^{Ol/L}$ is related to measured olivine CaO concentrations. This is particularly evident in some of the Walter (1998) experiments (e.g. experiments 30.10 and 30.14), where the 1 RMSE from equation (3) is totally accounted for by variations in the olivine CaO contents from experiments with similar quench liquid compositions, temperatures and pressures. Variable CaO in olivine is in part an analytical error associated with electron microprobe measurements; for example, a reported variation of $\pm 10\%$ in CaO concentration translates to a variation in $D_{CaO}^{Ol/L}$ of about $\pm 0{\cdot}002$, accounting for about half the RMSE in equation (3). Secondary Ca fluorescence from glass probably contributes to much of the scatter (M. Baker, personal communication, 2015), but we know of no way to correct for this. Figure 6b shows that values of $D_{CaO}^{Ol/L}$ obtained from this parameterization agree with those obtained from MELTS (Ghioro & Sack, 1995), Libourel (1999) and Herzberg & O'Hara (2002) to within the uncertainties stated above for melts having 8–18% MgO, a range that is appropriate for most parental magma compositions of interest (Supplementary Data Table A3).

An evaluation is now made of the suggestion by Feig *et al.* (2006) that H_2O affects the distribution of CaO between olivine and liquid. We begin this assessment using naturally occurring olivine-hosted melt inclusion studies (Fig. 7), and compare results to constraints from experimental petrology (Fig. 8). We use melt inclusion H_2O contents and major elements that were reported

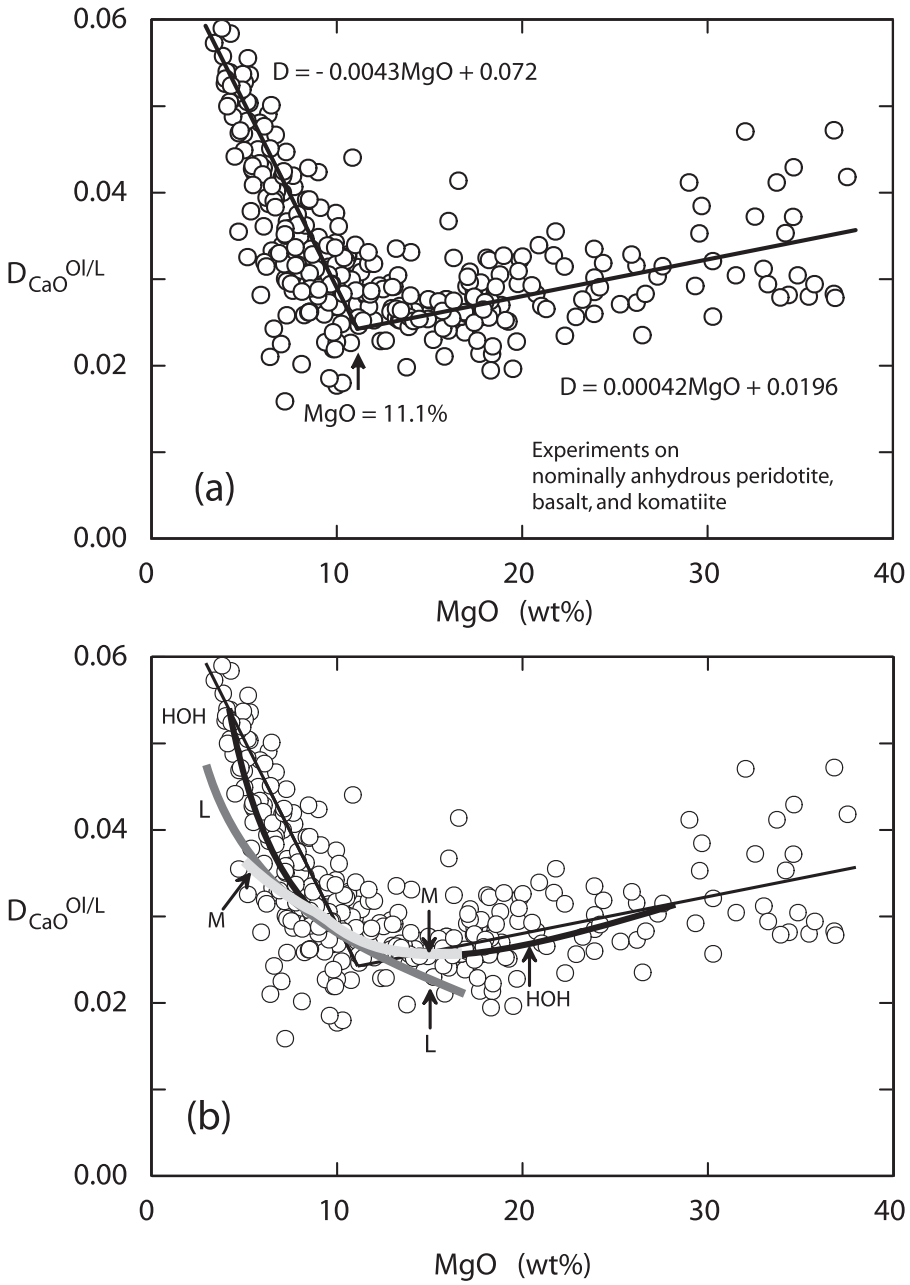

Fig. 6. The distribution of CaO between olivine and nominally volatile-free silicate liquid (i.e. $D_{CaO}^{Ol/L}$) as a function of melt MgO content, based on anhydrous melting experiments listed in the text. (a) A parameterization of low- and high-MgO data given by equations (2) and (3). For the high-MgO population most relevant to primary magmas, $D_{CaO}^{Ol/L}$ varies very little with MgO, demonstrating that it does not vary much with temperature. (b) Other parameterizations: HOH, Herzberg & O'Hara (2002); M, MELTS (Ghiorso & Sack, 1995); L, Libourel (1999). M and L are results of olivine and liquid compositions along a computed liquid line of descent for a primary magma containing 17% MgO; HOH is similar, but the higher MgO arises from olivine addition.

with their host olivines from different arc settings (Kamenetsky *et al.*, 2007; Portnyagin *et al.*, 2007*b*, 2014; Sadofsky *et al.*, 2008; Shaw *et al.*, 2008; Kelley *et al.*, 2010; Zimmer *et al.*, 2010; Cooper *et al.*, 2012). Other melt inclusion studies have been summarized by Plank *et al.* (2013), but many did not report olivine CaO content. We assume equilibrium between olivine and melt inclusions, and acknowledge complexities associated with melt inclusion zoning (Newcombe *et al.*, 2014). Most melt inclusions reveal variable degassing (e.g. Le Voyer *et al.*, 2014), so we accepted only compositions that provided maximum H_2O contents for each of the volcanoes (Plank *et al.*, 2013). Furthermore, for melt inclusions with nearly constant maximum H_2O contents but variable $D_{CaO}^{Ol/L}$, we accept only $D_{CaO}^{Ol/L}$ maxima as being most consistent with least degassed compositions. For example, a melt inclusion with a well-constrained H_2O content of 2% may plot at low $D_{CaO}^{Ol/L}$ and on the 6% H_2O isopleth if it degassed 4% H_2O and if there has been no diffusive re-equilibration of CaO between olivine and

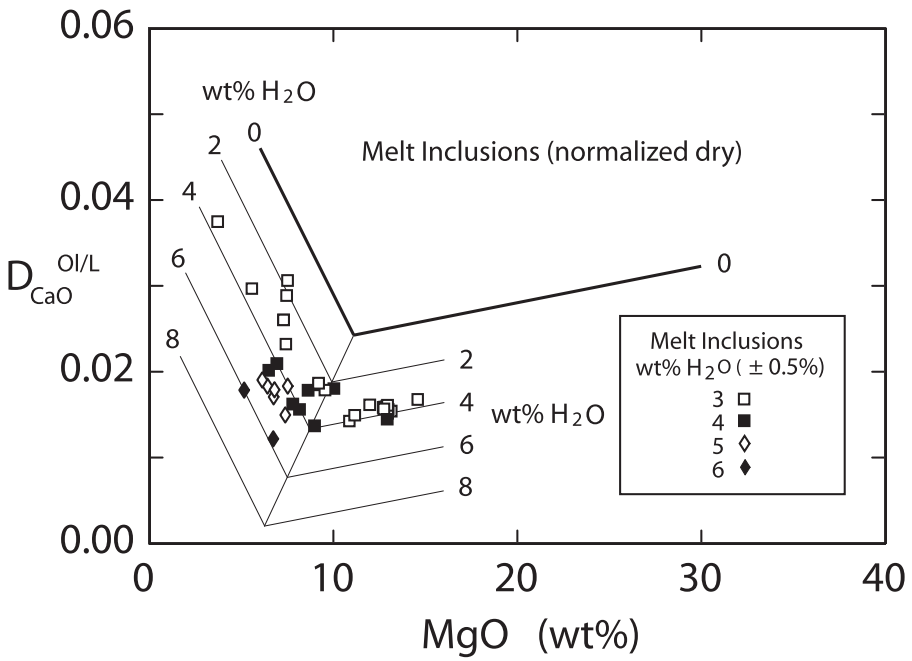

Fig. 7. The distribution of CaO between olivine and coexisting H_2O–melt inclusions as a function of the melt MgO content. Sources of melt inclusion data are given in the text. The 0 wt % H_2O isopleth is from Fig. 6a, and the 2–8 wt % H_2O isopleths are a parameterization of the effects of water on decreasing $D_{CaO}^{Ol/L}$ as given in the text. Melt inclusion data are divided between low- and high-MgO populations, separated by the diagonal line as defined by equation (7) in the text.

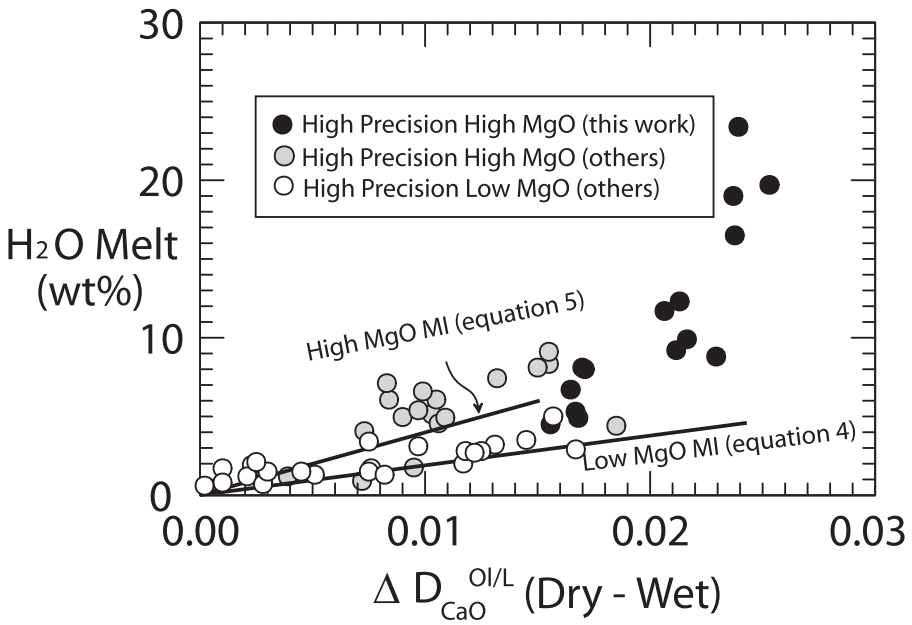

Fig. 8. Reported H_2O contents of experimental melts as a function of the difference in $D_{CaO}^{Ol/L}$ between dry and wet systems. $\Delta D_{CaO}^{Ol/L} = D_{CaO}^{Ol/L}$(dry) – $D_{CaO}^{Ol/L}$(wet), where $D_{CaO}^{Ol/L}$(dry) is derived from the parameterized nominally anhydrous results in Fig. 6a using equations (2) and (3). $D_{CaO}^{Ol/L}$(wet) is for experimental olivine and liquid compositions reported in the text. Low-MgO MI refers to melt inclusions and is obtained from equation (4), from Fig. 7. High-MgO MI refers to melt inclusions and is obtained from equation (5), also from Fig. 7.

melt. In this sense, the low diffusivity of Ca in olivine (Coogan *et al.*, 2005), when compared with that of H^+ (Hauri, 2002; Portnyagin *et al.*, 2008; Gaetani *et al.*, 2012; Bucholz *et al.*, 2013), has the potential to retain the memory of magmatic water that is otherwise lost by diffusion. Major elements were normalized to anhydrous, and $D_{CaO}^{Ol/L}$ for each olivine and its melt inclusion is shown in Fig. 7, together with the parameterized results for zero water [equations (2) and (3)]. Melt inclusion data confirm that the effect of H_2O is to decrease $D_{CaO}^{Ol/L}$, as

suggested by Feig *et al.* (2006), and we provide a preliminary linear parameterization. For the low-MgO melt population, data regression yields

$$H_2O = 188\Delta D_{CaO}^{OI/L} \quad (4)$$

where H_2O is the melt inclusion weight per cent water content. For the high-MgO melt population, regression yields

$$H_2O = 397\Delta D_{CaO}^{OI/L} \quad (5)$$

where H_2O is the melt inclusion weight per cent water content. In equations (4) and (5), the delta terms are defined as

$$\Delta D_{CaO}^{OI/L} = D_{CaO}^{OI/L}(dry) - D_{CaO}^{OI/L}(wet) \quad (6)$$

where $D_{CaO}^{OI/L}(dry)$ is derived from the parameterized nominally anhydrous results in Fig. 6a and given in equations (2) and (3) for the low- and high-MgO populations, respectively. In Fig. 7, the low- and high-MgO populations are separated by the line

$$D_{CaO}^{OI/L} = 0 \cdot 00462MgO - 0 \cdot 027. \quad (7)$$

Equations (4) and (5) describe the melt inclusion data to within ±0·7% H_2O at the 1σ level relative to the anhydrous system as described by equations (2) and (3). Propagating uncertainties in the anhydrous parameterizations, the total uncertainty in magmatic water inferred from $D_{CaO}^{OI/L}$ and MgO is ±1·4% H_2O (1σ) for the low-MgO population and ±1·8% H_2O (1σ) for the high-MgO population.

We now assess the influence of H_2O on the distribution of CaO between olivine and liquid from experimental data. The H_2O content of quench liquid in hydrous experiments has been measured by SIMS, FTIR, mass balance, and by difference (Hirose & Kawamoto, 1995; Müntener *et al.*, 2001; Parman & Grove, 2004; Feig *et al.*, 2006; Hauri *et al.*, 2006; Balta *et al.*, 2011; Tenner *et al.*, 2012; Nandedkar *et al.*, 2014). In addition, our database includes the nominally anhydrous results of Wasylenki *et al.* (2003), who measured 1·2% H_2O in one of their experiments; it is important to consider that the unintended entry of H_2O into nominally anhydrous experiments may contribute further to the uncertainty in the anhydrous parameterization given in Fig. 6a. As with anhydrous experiments, we note large uncertainties in the reported CaO contents of olivine in some cases, and accept only results with reported variations of ±10%. Quench melt compositions reported by Tenner *et al.* (2012), from synthetic peridotite KLB-1 + H_2O, were used in conjunction with coexisting olivines that we reanalyzed by high-precision electron microprobe analysis; data are given in Supplementary Data Table A2. The root mean square error of measured olivine CaO in the Tenner *et al.* (2012) experiments ranges from ±5 to 13% relative; this is in contrast to ±1·5% in our San Carlos olivine standard, which was measured over 300 times before, during, and after each analytical routine, to correct for machine drift. Of the elements measured, Ca invariably displays the largest uncertainty; some of this may be attributed to secondary Ca fluorescence, but we have measured significant heterogeneity within the cores of single olivine crystals. We conclude that equilibrium was only partially achieved with respect to CaO distribution between olivine and liquid in experiments run for long durations and in the presence of H_2O.

Experimental results are displayed as the amount of H_2O in the melt as a function of the difference between $D_{CaO}^{OI/L}$ in the nominally anhydrous system and $D_{CaO}^{OI/L}$ in the hydrous experiments (i.e. $\Delta D_{CaO}^{OI/L}$; Fig. 8). For reference, the experiments are compared with equations (4) and (5) from the melt inclusion studies. In general, there is agreement with melt inclusion studies that the effect of magmatic H_2O is to decrease $D_{CaO}^{OI/L}$, thereby increasing the difference with respect to the dry system (i.e. $\Delta D_{CaO}^{OI/L}$). Experimental melt compositions having low MgO (Feig *et al.*, 2006; Nandedkar *et al.*, 2014) yield $D_{CaO}^{OI/L}$ and H_2O contents that best agree with melt inclusion studies. In contrast, high-MgO experimental melt compositions display a considerable range of H_2O contents at constant $\Delta D_{CaO}^{OI/L}$, much greater than that of melt inclusions, and this precludes their use as a geohygrometer. One potential issue with experiments is that samples could be compromised by inadvertent CO_2 contamination, as a result of the use of graphite capsules in high-pressure experiments. Figure 9 shows that CO_2 can affect $D_{CaO}^{OI/L}$ in a manner similar to H_2O, based on nominally anhydrous carbonated experimental data reported by Dasgupta *et al.* (2007, 2013). In general, volatiles suppress $D_{CaO}^{OI/L}$, and at present we cannot distinguish CO_2 from H_2O. Tenner *et al.* (2012) corrected the melt compositions for CO_2, but we use their uncorrected melt compositions for purposes of consistency and comparison with other studies for which no such corrections were provided. Melts synthesized in all nominally anhydrous and carbonated experiments probably contain both CO_2 and H_2O, and melts of all hydrous experiments probably have some amount of CO_2. Even small amounts of each volatile can substantially lower $D_{CaO}^{OI/L}$, and we know of no way to deconvolve the effects of CO_2 from H_2O with confidence. Therefore, we rely exclusively on studies of naturally occurring olivine-hosted melt inclusion as a means to calibrate the olivine hygrometer.

APPLICATION OF THE OLIVINE GEOHYGROMETER

Olivines and whole-rocks

A prediction can be made of magmatic H_2O concentrations using the composition of olivine in equilibrium with its parental magma as inferred from whole-rock compositions. In general, whole-rock compositions are not in equilibrium with olivine, and it is necessary to add olivine to or subtract it from the most primitive rock to compute the CaO and MgO content of the parental

magma in equilibrium with measured olivines with the highest Mg-numbers. This procedure is discussed in the Supplementary Data, and results are given in Supplementary Data Table A3. We work exclusively with high-precision olivine analyses from Hawaii, Ontong Java Plateau, Gorgona komatiites, and Archean komatiites reported by Sobolev *et al.* (2007). For Siqueiros MORB and subduction zones, we use high-precision olivine data reported in this study (Supplementary Data Table A1). H_2O contents are obtained using equations (1)–(6), and results from a wide range of geological occurrences are shown in Fig. 10.

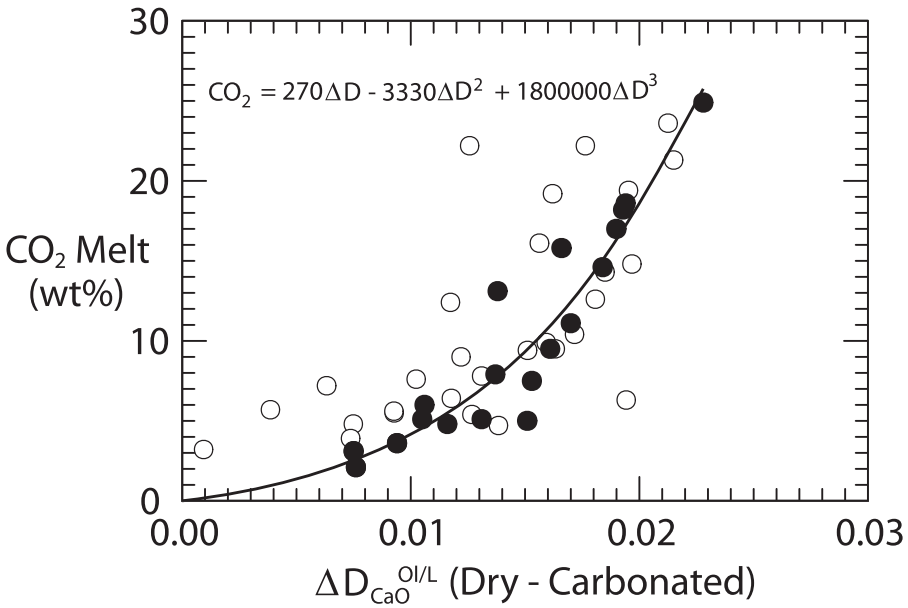

Fig. 9. Reported CO_2 contents of experimental melts as a function of the difference in $D_{CaO}^{Ol/L}$ between a dry and carbonated system. $\Delta D_{CaO}^{Ol/L} = D_{CaO}^{Ol/L}$(dry) – $D_{CaO}^{Ol/L}$(carbonated), where $D_{CaO}^{Ol/L}$(dry) is computed from equations (2) and (3). Filled circles are data from Dasgupta *et al.* (2007) and the regression is based on these data; open circles are data from Dasgupta *et al.* (2013).

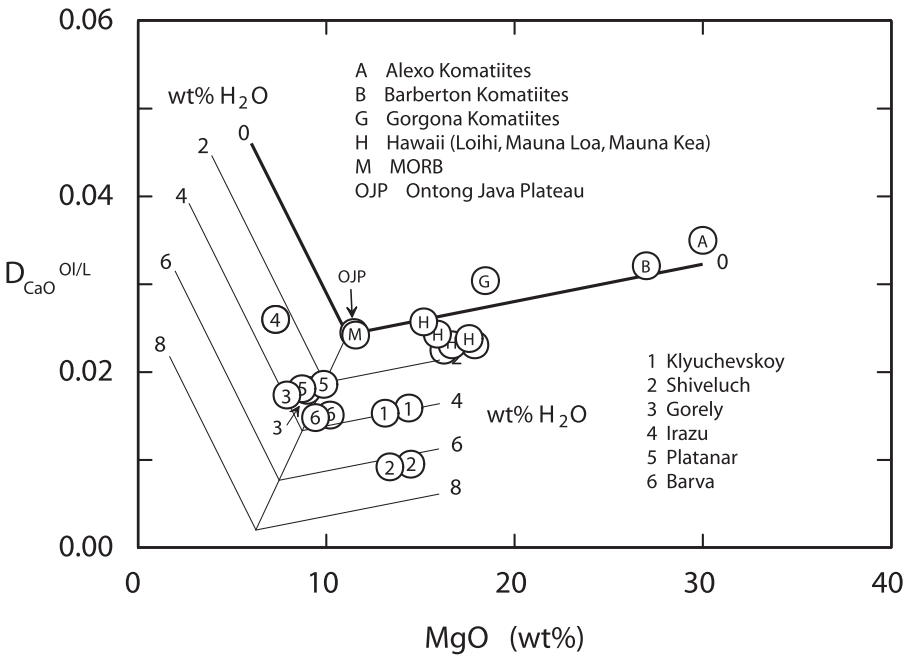

Fig. 10. Inferred magmatic H_2O contents in different tectonic environments based on the CaO content of an olivine grain that was in equilibrium with a parental magma for which the MgO and CaO contents are known. Parental magmas were estimated by incremental olivine addition to and sometimes subtraction from lava whole-rock or glass compositions until equilibrium was achieved with olivines having the highest Mg-numbers (Supplementary Data). $D_{CaO}^{Ol/L}$ and MgO contents for parental magmas are given in Supplementary Data Table A3. Olivine CaO contents used to obtain $D_{CaO}^{Ol/L}$ were obtained from high-precision data for Hawaii, Ontong Java Plateau, Gorgona komatiites, and Archean komatiites (Sobolev *et al.*, 2007), and high-precision data for MORB and subduction zones reported in this study (Supplementary Data Table A1).

By applying the olivine geohygrometer, we estimate low magmatic H_2O for lavas containing high Ca contents in olivine (e.g. Fig. 2). This result is relevant for MORB, the Ontong Java Plateau, Hawaii, and komatiites from Gorgona and various Archean occurrences (Fig. 10). We calculate 0·1% H_2O for Siqueiros MORB sample D-20-15, in good agreement with 0·04–0·12% H_2O from measurements on olivine-hosted melt inclusions (Saal *et al.*, 2002). For the Ontong Java Plateau sample 1187, we obtain 0% H_2O, in good agreement with 0·20% measured by Roberge *et al.* (2005). Calculated water contents for Loihi, Mauna Loa and Mauna Kea on Hawaii range from zero to 1·6%; they are mostly higher than measured H_2O contents from olivine-hosted melt inclusions (Hauri, 2002), but within the uncertainty of our geohygrometer. Archean komatiites from Alexo in the Superior Province and the Komati Formation of the Barberton greenstone belt are estimated to be dry magmas, in contrast to wet magmas that have been inferred in subduction zones (Parman *et al.*, 1997). However, there is ambiguity with this interpretation because the komatiites may also have been volatile-rich magmas that degassed before olivine crystallized in surface flows. If hydrous melting in subduction zones was important in Archean komatiite petrogenesis, then it must have been fundamentally different from that at the present time as indicated by the contrasting contents of Ca in olivine (Fig. 2).

The CO_2 contents of subduction zone volatiles are generally low (e.g. Manning, 2004; Kelley *et al.*, 2010; Plank *et al.*, 2013; Aiuppa *et al.*, 2014; Mironov *et al.*, 2015). Therefore, low $D_{CaO}^{Ol/L}$ should be predominantly influenced by H_2O. In general, the estimated magmatic H_2O concentration ranges from 3 to 4 wt % (Fig. 10) at the Kamchatka and Central American arcs, which agrees with H_2O maxima from melt inclusion studies (Plank *et al.*, 2013).

We calculate 3·9% H_2O for primitive melts in equilibrium with olivines having an Mg-number of 91·9 from the Klyuchevskoy volcano, which is in good agreement with recent estimations of the water content of Klyuchevskoy parental magmas: 3·5 wt % from melt inclusion studies (Mironov & Portnyagin, 2011) and 3·9–4·9 wt % from the hydration-driven homogenization of olivine-hosted melt inclusions (Mironov *et al.*, 2015). Numerous Klyuchevskoy melt inclusion studies (e.g. Portnyagin *et al.*, 2007*b*; Auer *et al.*, 2009) have reported a very wide range of melt inclusion water contents—from less than 1 wt % to 7·1 wt %. Low melt inclusion water content is explained by magma and/or melt inclusion degassing, whereas 7·1% H_2O has been explained by magmatic H_2O accumulation as an incompatible component during fractional crystallization (Mironov & Portnyagin, 2011).

For the Shiveluch volcano located north of Klyuchevskoy, we calculate 6·4% H_2O contents for parental melts in equilibrium with olivine having an Mg-number of 92·5. This high value of H_2O content for the Shiveluch parental magma may help to explain the existence of high-magnesium (MgO is ~11 wt %) basaltic rocks bearing phlogopite and amphibole (Volynets *et al.*, 1997; Ponomareva *et al.*, 2007; Gorbach & Portnyagin, 2011). Possible contributions to the high water content in Shiveluch parental magmas are lower mantle wedge temperatures, less peridotite material assimilated by hydrous eclogite melts, and a higher relative contribution of water from the slab (Portnyagin *et al.*, 2007*a*).

We calculate 3·0% H_2O for primitive melts in equilibrium with olivines having an Mg-number of 86·3 from the Gorely volcano, which is in good agreement with three independent estimations (2·8–3·0 wt % of H_2O) reported in Gavrilenko *et al.* (2016).

In the Central American arc, 3·5% H_2O is inferred for the Barva volcano and 2·0% H_2O is inferred for the Platanar volcano. For Irazú, our geohygrometer yields 2·7 wt % H_2O, in good agreement with 2·8–3·2 wt % reported by Benjamin *et al.* (2007) from melt inclusions in the most primitive olivines.

Olivines and melt inclusions

Another way to infer magmatic water is by application of our olivine geohygrometer to the compositions of olivines and their melt inclusions that have been corrected for olivine crystallization. Results for several well-described cases are given in Fig. 11. Sobolev *et al.* (2011) provided data for Mauna Loa and the most MgO-rich melt inclusions are consistent with about 1·2% H_2O; low MgO contents that indicate higher H_2O contents are artifacts of incorrectly reconstructing olivine crystallization along the melt inclusion walls. Inferred 1·2% H_2O for the high-MgO Mauna Loa population is similar to that obtained from whole-rocks (Fig. 11), and it is higher than the 0·35% maxima reported by Hauri (2002) and the 0·37% mean reported by Sobolev *et al.* (2011). Although this difference is well within the uncertainty of our geohygrometer, it may also indicate that the low diffusivity of Ca in olivine is retaining the memory of H^+ that was lost by diffusion. Likewise, ~1% H_2O inferred for melt inclusions from the Gudchikhinsky Formation

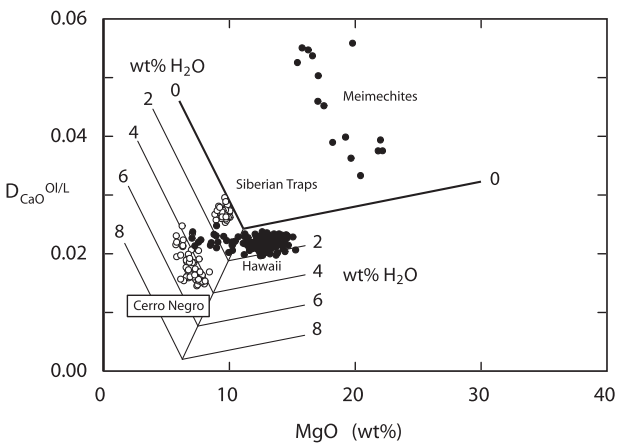

Fig. 11. Inferred magmatic H_2O contents in different tectonic environments based on olivines in equilibrium with their melt inclusions.

of the Siberian Traps (Fig. 11) is higher than the 0·03–0·25% reported by Sobolev *et al.* (2009*a*).

Application of our geohygrometer to the compositions of olivine-hosted melt inclusions from the Cerro Negro volcano in Nicaragua, compiled by Portnyagin *et al.* (2014), yields ~4–6% H_2O (Fig. 11). This range is higher than but overlapping with 0·5–6% H_2O measured by SIMS and FTIR (Roggensack *et al.*, 1997; Roggensack, 2001; Wehrmann *et al.*, 2011; Portnyagin *et al.*, 2014). Again, the low diffusivity of Ca in olivine may be retaining the memory of H^+ that was lost by diffusion in some cases.

Our geohygrometer fails to explain the partitioning of CaO between melt inclusions and their host olivines for meimechites (Sobolev *et al.*, 2009*b*; Fig. 11). Meimechites are ultramafic, potassium-rich and silica-poor volcanic rocks restricted to northern Siberia (Arndt *et al.*, 1995; Sobolev *et al.*, 2009*b*). Olivines in meimechites are anomalously high in CaO, which explains the high $D_{CaO}^{Ol/L}$ at around 20% MgO relative to our geohygrometer (Fig. 11). The meimechites also have unusually high CaO/Al_2O_3, in the 1·5–2·5 range, owing mostly to low Al_2O_3 rather than high CaO (Sobolev *et al.*, 2009*b*). We expect that the meimechite misfit indicates shortcomings with the ability of using MgO as the sole adjustable parameter to describe the partitioning of CaO between olivine and melt.

EVIDENCE FOR HYDRATION AND DEHYDRATION RECORDED BY OLIVINES FROM KLYUCHEVSKOY AND SHIVELUCH VOLCANOES

For Klyuchevskoy, the gradual but substantial decrease in Ca in the core of olivine grain 26, from 1450 ppm at the center to 1060 ppm at the rim contact, is not correlated with changes in Mg, Fe, Ni, and Mn (Fig. 4). We now test and reject a number of hypotheses to explain these observations.

(1) Olivine grain 26 was a phenocryst that grew during partial crystallization of olivine and/or low-Ca pyroxene. This scenario predicts that the grain should exhibit normal zoning with Ca increasing and Mg-number decreasing from core to rim, but this is not observed. However, we might imagine that such zoning did occur during crystallization, but the faster diffusing elements such as Mg, Fe, Mn, and Ni were subsequently completely re-equilibrated, whereas the slower diffusing Ca was only partially equilibrated. We can discount this explanation because olivine grain 26 is not zoned in even slower diffusing elements such as phosphorus and aluminum, data that will be reported in a subsequent and more detailed study.

(2) Olivine grain 26 was a phenocryst that initially grew from a high-Ca magma, and subsequently mixed into a low-Ca magma. The faster diffusing elements such as Mg, Fe, Mn, and Ni were subsequently completely re-equilibrated, whereas the slower diffusing Ca was only partially equilibrated. Again, this is not likely because the strong Ca zoning is not revealed in the slow-diffusing elements P and Al.

We propose that the core–rim decrease in Ca content in olivine grain 26 may reflect time-progressive H_2O addition, and predict how this hypothesis can be tested. In the absence of regularly spaced melt inclusions distributed from core to rim, we assume that the parental magma contains 8·7% CaO (Supplementary Data Table A3). Reference to our geohygrometer (Fig. 10) indicates that the core of grain 26 could have formed in response to increased magmatic H_2O, from 0·9 to 3·5%, as shown in Fig. 12. This was calculated from $D_{CaO}^{Ol/L}$ using core-to-rim olivine CaO contents (Fig. 4b) and an assumed parental magma having 8·7% CaO (Supplementary Data Table A3). Magmatic H_2O contents were calculated from equations (1), (3), (5) and (6). Olivine H_2O contents were calculated from olivine–melt H_2O partition coefficients of 0·0007 (Tenner *et al.*, 2009; Le Voyer *et al.*, 2014) and 0·0015 (Hauri *et al.*, 2006). This range of predicted H_2O contents will represent an upper bound if the slab melts or fluids are deficient in CaO when compared with our assumed parental magma composition. Furthermore, this assumed constant magmatic Ca content will probably compromise inferences about predicted H_2O contents to an at present unknown extent; our model needs to be tested and subject to falsification by core–rim analyses of H_2O contents using SIMS analysis. In the absence of SIMS data, our olivine geohygrometer predicts that olivine is capturing in its Ca content the time-progressive entry of H_2O from the subducted slab. Olivine hydration may occur in the mantle wedge during convective corner flow, from distal drier parts to proximal wetter regions above the slab. The similarity of ~1000 ppm Ca at the Klyuchevskoy rim contact with primitive olivines from Central America (Fig. 2b) may indicate that our inferred

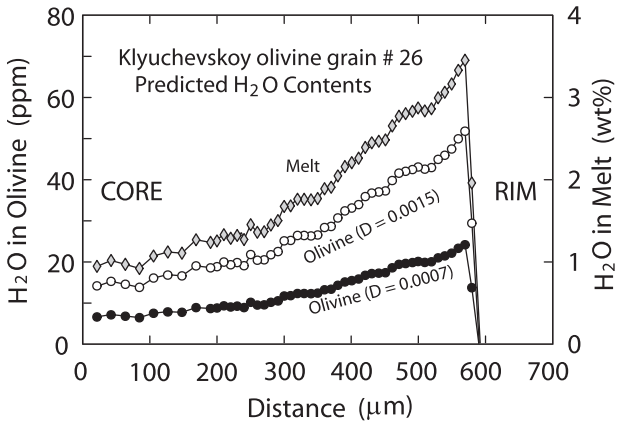

Fig. 12. Predicted H_2O contents of olivine grain 26 from Klyuchevskoy volcano and equilibrium melt compositions. $D_{CaO}^{Ol/L}$ was calculated from core to rim using olivine CaO contents given in Fig. 4b and a parental magma having 8·67% CaO (Supplementary Data Table A3). Magmatic H_2O contents were calculated from equations (1), (3), (5) and (6). Olivine H_2O contents were calculated using olivine–melt H_2O partition coefficients of 0·0007 (Tenner *et al.*, 2009; Le Voyer *et al.*, 2014) and 0·0015 (Hauri *et al.*, 2006).

3·5% H_2O is a common global feature, in agreement with conclusions drawn by Plank *et al.* (2013).

In contrast to cores, Klyuchevskoy olivine rims record an increase in Ca concentration, as most vividly illustrated within grain 26 (Fig. 4b). This is not an artifact of secondary Ca fluorescence from glass because the olivines are grain mounts. We interpret the increased Ca in olivine rims as a response to dehydration of the host magma during ascent. The abrupt drop in Mg-number and Ni content in the olivine rims also reflects the influence of crystallization. Portnyagin *et al.* (2014) similarly provided evidence for dehydration during crystallization of clinopyroxene for the Cerro Negro volcano, and that this drove down CaO in the derivative magmas. For Klyuchevskoy, it can be shown that olivine has an Mg-number of ~88 when clinopyroxene starts to crystallize along the LLD at 8–10% MgO, much higher than olivine rim compositions (Fig. 4a). It might be counterintuitive, but dehydration can drive up the Ca contents of the olivine rims even when clinopyroxene crystallization drives down the Ca contents of the derivative magmas. In general, olivine rims record dehydration during decompression crystallization.

Shiveluch olivine grain 10 is similar to Klyuchevskoy olivine in that it exhibits Ca-related evidence for hydration in the core, as well as dehydration in the rim (Fig. 5b); however, absolute Ca contents are much lower in Shiveluch, indicating that the olivines originated from more H_2O-rich melts or fluids. If we assume a parental Shiveluch magma with 15·4% MgO and 7·5% CaO (Supplementary Data Table A3), then reference to our geohygrometer indicates that the core of Shiveluch grain 10 formed in response to an increase of H_2O, from 4·8 to 6·5%; using a partition coefficient of 0·0015 for H_2O between olivine and melt (Hauri *et al.*, 2006), the olivine core in grain 10 is expected to contain 72–98 ppm H_2O. This range would drop by half using an olivine–melt partition coefficient of 0·0007 from Tenner *et al.* (2009) and Le Voyer *et al.* (2014). These predicted high water contents can be falsified with SIMS analysis.

We find no relationship between inferred magmatic H_2O content and olivine Ni content. For example, wet olivine cores from Shiveluch have ~3000 ppm Ni (Fig. 5c), which is similar to 2800–3100 ppm Ni in olivine in mantle peridotite (Herzberg *et al.*, 2013), and Ni in olivine from dry Siqueiros MORB and other anhydrous partial melts of peridotite (Herzberg, 2011). Furthermore, variations in olivine core Ni contents from the Klyuchevskoy volcano (Fig. 4c) do not correlate with variations in Ca concentration. However, 1600 ppm Ni in grain 26 is notably very low, perhaps reflecting the participation of sulfide or some other phase (Li *et al.*, 2013) or S-bearing metasomatic fluids and melts in subduction environments (Bataleva *et al.*, 2016). Low olivine Ni contents have also been reported in olivines from dunites in mantle peridotite, and these can form by the dissolution and replacement of pyroxene in melt channels (Kelemen *et al.*, 1995, 1997; Suhr *et al.*, 2003; Batanova & Savelieva, 2009). In the melt–rock reaction model, olivine replaces pyroxenes according to the reaction pyroxene + liquid → olivine + spinel + liquid (Kelemen *et al.*, 1997). Comparable with Kamchatka olivine grain 26 are olivines in dunites from the Luobusa ophiolite, the Oman ophiolite (1257–1885 ppm Ni; Koga *et al.*, 2001), and dunite xenoliths from Shiveluch volcano in Kamchatka (1570 ppm Ni; Bryant *et al.*, 2007). It is therefore possible that Klyuchevskoy olivine grain 26 originated by melt–rock reaction in the mantle. Of course, we cannot tell whether the olivine grain was plucked from a melt channel that contained olivine as a sole crystalline phase, or if it was olivine-rich peridotite. Also, we have no way to evaluate the depth at which melt–rock reaction occurred below Kamchatka.

Olivine grains from Klyuchevskoy and Shiveluch have Mg-numbers ranging from 90 to 93 (Figs 4 and 5), similar to those reported by Kamenetsky *et al.* (2006) from Kamchatka and other subduction zone occurrences. One explanation is that these olivines crystallized as phenocrysts from primitive magmas; problems with this interpretation were discussed above. Alternatively, the olivine grains might have been in equilibrium with primary magmas in the partial melting region, as we indicate in Figs 4 and 5, and have nothing to do with partial crystallization. This hypothesis is consistent with data from Klyuchevskoy olivine grains 13 and 26, which appear to have exotic origins because they display diffusion-controlled radial offsets in Mg-number, Ni, and Ca (Fig. 4). We attribute the offset signature to a process where entire grains were plucked from the melting region and the rims recorded diffusion profiles that formed by partial re-equilibration with their host magmas during ascent in the volcano conduit. Furthermore, other researchers have considered the possibility that not all magmatic olivines originated by partial crystallization in the crust (Plank *et al.*, 2013; Ruprecht & Plank, 2013). As discussed in the preceding paragraph a mantle origin by melt–rock reaction for Klyuchevskoy olivine grain 26 would explain the low Ni content. In the paragraph that follows, we assume that the olivine grains from Klyuchevskoy and Shiveluch volcanoes originated in deep partial melting regions in the mantle; but we acknowledge that more work is needed to determine if there are geodynamic impediments related to the export of olivines from this region.

The mantle wedge below the Central Kamchatka Depression is probably dominated by a peridotite lithology, as indicated by the primitive olivines with high Mg-numbers and low Ni contents (Figs 4 and 5). This may seem paradoxical because siliceous slab melts and fluids are likely to react with wedge peridotite, thereby transforming it to pyroxenite (e.g. Kelemen *et al.*, 2003; Portnyagin *et al.*, 2007*a*; Straub *et al.*, 2008, 2011). Furthermore, the indelible signature of many pyroxenite melts is that they crystallize olivines with elevated Ni contents (Kelemen *et al.*, 1998; Sobolev *et al.*, 2005, 2007; Herzberg, 2011; Vidito *et al.*, 2013), as shown clearly by examples from the Mexican Volcanic Belt

(Straub *et al.*, 2008, 2011) and Irazú (Ruprecht & Plank, 2013). However, Ni-rich olivines are not a typical feature of Klyuchevskoy and Shiveluch volcanoes. The dominance of peridotite source melting below the Central Kamchatka Depression might indicate that the high magmatic H_2O contents originated by low-SiO_2 slab dehydration rather than by high-SiO_2 slab melting. Alternatively, pyroxenite could have formed in abundance at some point below the Central Kamchatka Depression, but was subsequently melted out. There is great potential for using olivine chemistry to understand in more detail the provenance of olivine and magmatic H_2O in subduction zones.

DISCUSSION AND CONCLUSIONS

High-precision electron microprobe analyses were obtained on olivine grains from the Siqueiros Transform (East Pacific Rise); Klyuchevskoy, Shiveluch and Gorely volcanoes in the Kamchatka Arc; and the Irazú, Platanar and Barva volcanoes of the Central American Arc. Calcium contents of these subduction zone olivines are lower than those for olivines from modern MORB, Archean komatiites, and Hawaii. A role for magmatic H_2O is likely for subduction zone olivines, and we have explored the suggestion by Feig *et al.* (2006) that H_2O has affected the partitioning of CaO between olivine and silicate melt. We provide a calibration of CaO partitioning between olivine and its equilibrium melt as a geohygrometer and show that it is necessarily preliminary, in part because many nominally anhydrous experiments are inadvertently volatile-bearing, and it is difficult to deconvolve the effects of H_2O and CO_2 in volatile-bearing experiments. Equally of concern is that experimental olivine Ca contents were probably compromised by secondary Ca fluorescence and low Ca diffusivity. In principle, the low diffusivity of Ca in olivine (Coogan *et al.*, 2005), when compared with that of H^+ (Hauri, 2002; Portnyagin *et al.*, 2008; Gaetani *et al.*, 2012; Bucholz *et al.*, 2013), might help to retain the memory of magmatic water that is otherwise lost by diffusion and degassing. We have circumvented some of these problems by comparing melting experiments from nominally anhydrous systems with minimally degassed H_2O contents of olivine-hosted melt inclusions. Melt inclusions can be heterogeneous and equilibrium with host olivines may be problematic, and the uncertainties are large. However, application of our geohygrometer typically yields 3–4 wt % magmatic H_2O for the Kamchatka and Central American arcs for olivines having ~1000 ppm Ca, which agrees with H_2O maxima from melt inclusion studies (Plank *et al.*, 2013); Cerro Negro and Shiveluch volcanoes are exceptions, with about 6% H_2O. Our geohygrometer is by no means a replacement for more accurate methods of H_2O analysis, but it has the advantage of applicability in cases where olivine-hosted melt inclusions do not exist. Additionally, application of the geohygrometer to core–rim olivine Ca analyses has the potential to reveal changes in magmatic H_2O, as revealed by the Klyuchevskoy and Shiveluch volcanoes. Even if olivine-hosted melt inclusions do exist, it is not likely that they have core–rim distributions that will permit an evaluation of variations in magmatic H_2O by SIMS analysis. In the ideal case, SIMS analysis of melt inclusions can be complemented by the Ca content of olivine, to yield a more complete assessment of the role of water in subduction zones.

High-precision electron microprobe analyses with 10–20 μm spatial resolution on some olivine grains from Klyuchevskoy and Shiveluch show a decrease in Ca content from core centers to the rim contacts. Our geohygrometer indicates that the olivine grains may record entry of magmatic H_2O. Furthermore, high Mg-numbers and Ni contents indicate that these are mantle olivines, and the inferred H_2O may record entry from the slab to the mantle wedge. In contrast, olivine rims probably record decompression dehydration during crystallization in the volcano conduit or crust. Variations in olivine Mg-number and Ca contents (e.g. Fig. 2b) record a complex history of partial melting and crystallization, H_2O entry and degassing, and diffusion. We suggest that zoning of Ca in olivine from subduction zone lavas may provide the first petrological record of temporal changes that occur during hydration of the mantle wedge and dehydration during magma ascent, and we predict olivine H_2O contents that can be tested by SIMS analysis.

ACKNOWLEDGEMENTS

We thank Philip Kyle for providing Shiveluch basaltic tephras, and Michael Perfit for providing samples of MORB from the Siqueiros Transform. We are grateful to Nina Søager for critical comments, and to Maxim Portnyagin for discussions. Special thanks go to Michael Baker for comments that greatly improved the paper. Marjorie Wilson is thanked for editorial suggestions. We are grateful to Maxim Portnyagin, Philipp Ruprecht and Alex Sobolev for critical reviews that helped to improve this paper.

FUNDING

M.G. thanks the International Fulbright Science and Technology Award for financial support of the study in 2011–2014, and Graduate School of Rutgers University, New Brunswick for financial support of the study in 2015–2016. M.G. also acknowledges support from the Far East Branch of the Russian Academy of Sciences grants 12-III-A-08-166 and 15-I-1-025. A.O. acknowledges support from the Far East Branch of the Russian Academy of Sciences, grant 15-I-2-069, and Russian Foundation of Basic Research, grant 15-05-05502.

SUPPLEMENTARY DATA

Supplementary data for this paper are available at *Journal of Petrology* online.

REFERENCES

Aiuppa, A., Robidous, P., Tamburello, G., Conde, V., Galle, B., Avard, G., Bagnato, E., De Moor, J. M., Martinez, M. & Muñóz, A. (2014). Gas measurements from the Costa Rica–Nicaragua volcanic segment suggest possible along-arc variations in volcanic gas chemistry. *Earth and Planetary Science Letters* **407**, 134–147.

Almeev, R. R., Kimura, J.-I., Ariskin, A. A. & Ozerov, A. Y. (2013). Decoding crystal fractionation in calc-alkaline magmas from Bezymianny Volcano (Kamchatka, Russia) using mineral and bulk rock compositions. *Journal of Volcanology and Geothermal Research* **263**, 141–171.

Alvarado, G. E. & Carr, M. J. (1993). The Platanar–Aguas Zarcas volcanic centers, Costa Rica: spatial–temporal association of Quaternary calc-alkaline and alkaline volcanism. *Bulletin of Volcanology* **55**, 443–453.

Alvarado, G. E., Carr, M. J., Turrin, B. D., Swisher, C. C., Schmincke, H.-U. & Hudnut, K. W. (2006). Recent volcanic history of Irazú volcano, Costa Rica: Alternation and mixing of two magma batches, and pervasive mixing. In: Rose, W. I., Bluth, G. J. S. & Carr, M. J. *et al.* (eds) *Volcanic Hazards in Central America. Geological Society of America, Special Papers* **412**, 259–276.

Ariskin, A. A., Barmina, G. S., Ozerov, A. Y. & Nielsen, R. L. (1995). Genesis of high-alumina basalts from Klyuchevskoi volcano. *Petrology* **3**, 449–472.

Arndt, N. T., Lehnert, K. & Vasil'ev, Y. (1995). Meimechites: highly magnesian lithosphere-contaminated alkaline magmas from deep subcontinental mantle. *Lithos* **34**, 41–59.

Auer, S., Bindeman, I., Wallace, P., Ponomareva, V. & Portnyagin, M. (2009). The origin of hydrous, high-δ^{18}O voluminous volcanism: diverse oxygen isotope values and high magmatic water contents within the volcanic record of Klyuchevskoy volcano, Kamchatka, Russia. *Contributions to Mineralogy and Petrology* **157**, 209–230.

Baker, M. B. & Stolper, E. M. (1994). Determining the composition of high-pressure melts using diamond aggregates. *Geochimica et Cosmochimica Acta* **58**, 2811–2827.

Balta, J. B., Asimow, P. D. & Mosenfelder, J. L. (2011). Hydrous, low-carbon melting of garnet peridotite. *Journal of Petrology* **52**, 2079–2105.

Bataleva, Y. V., Palyanov, Y. N., Borzdov, Y. M. & Sobolev, N. V. (2016). Sulfidation of silicate mantle by reduced S-bearing metasomatic fluids and melts. *Geology* **44**, 271–274.

Batanova, V. G. & Savelieva, G. N. (2009). Melt migration in the mantle beneath spreading zones and formation of replacive dunites: a review. *Russian Geology and Geophysics* **50**, 763–778.

Beattie, P., Ford, C. & Russell, D. (1991). Partition coefficients for olivine–melt and orthopyroxene–melt systems. *Contributions to Mineralogy and Petrology* **109**, 212–224.

Benjamin, E., Plank, T., Wade, J. A., Kelley, K. A., Hauri, E. H. & Alvarado, G. E. (2007). High water contents in basaltic magmas from Irazú Volcano, Costa Rica. *Journal of Volcanology and Geothermal Research* **168**, 68–92.

Braitseva, O. A., Melekestsev, I. V., Ponomareva, V. V. & Sulerzhitsky, L. D. (1995). Ages of calderas, large explosive craters and active volcanoes in the Kuril–Kamchatka region, Russia. *Bulletin of Volcanology* **57**, 383–402.

Bryant, J. A., Yogodzinski, G. M. & Churikova, T. G. (2007). Melt–mantle interactions beneath the Kamchatka arc: Evidence from ultramafic xenoliths from Shiveluch volcano. *Geochemistry, Geophysics, Geosystems* **8**, Q04007.

Bucholz, C. E., Gaetani, G. A., Behn, M. D. & Shimizu, N. (2013). Post-entrapment modification of volatiles and oxygen fugacity in olivine-hosted melt inclusions. *Earth and Planetary Science Letters* **374**, 145–155.

Carr, M. J., Feigenson, M. D., Bolge, L. L., Walker, J. A. & Gazel, E. (2013). RU CA Geochem v.3, a database and sample repository for Central American volcanic rocks at Rutgers University. Earth Chemistry Library, http://dx.doi.org/10.1594/IEDA/100409.

Chakraborty, S. (2010). Diffusion coefficients in olivine, wadsleyite and ringwoodite. In: Zhang, Y. & Cherniak, D. J. (eds) *Diffusion in Minerals and Melts.Mineralogical Society of America and Geochemical Society, Reviews in Mineralogy and Geochemistry* **72**, 603–639.

Chalot-Prat, F., Falloon, T. J., Green, D. H. & Hibberson, W. O. (2010). An experimental study of liquid compositions in equilibrium with plagioclase + spinel lherzolite at low pressures. *Journal of Petrology* **51**, 2349–2376.

Chalot-Prat, F., Falloon, T. J., Green, D. H. & Hibberson, W. O. (2013). Melting of plagioclase + spinel lherzolite at low pressures (0·5 GPa): an experimental approach to the evolution of basaltic melt during mantle refertilization at shallow depths. *Lithos* **172–173**, 61–80.

Canil, D. (1992). Orthopyroxene stability along the peridotite solidus and the origin of cratonic lithosphere beneath southern Africa. *Earth and Planetary Science Letters* **111**, 83–95.

Coogan, L. A., Hain, A, Stahl, S. & Chakraborty, S. (2005). Experimental determination of the diffusion coefficient for calcium in olivine between 900 °C and 1500 °C. *Geochimica et Cosmochimica Acta* **69**, 3683–3694.

Coogan, L. A., Saunders, A. D. & Wilson, R. N. (2014). Aluminum-in-olivine thermometry of primitive basalts: Evidence of an anomalously hot mantle source for large igneous provinces. *Chemical Geology* **368**, 1–10.

Cooper, L. B., Ruscitto, D. M., Plank, T., Wallace, P. J., Syracuse, E. M. & Manning, C. E. (2012). Global variations in H_2O/Ce: 1. Slab surface temperatures beneath volcanic arcs. *Geochemistry, Geophysics, Geosystems* **13**, Q03024.

Dasgupta, R., Hirschmann, M. M. & Smith, N. D. (2007). Partial melting experiments of peridotite CO_2 at 3 GPa and genesis of alkalic ocean island basalts. *Journal of Petrology* **48**, 2093–2124.

Dasgupta, R., Mallik, A., Tsuno, K., Withers, A. C., Hirth, G. & Hirschmann, M. M. (2013). Carbon-dioxide-rich silicate melt in the Earth's upper mantle. *Nature* **493**, 211–215.

Davis, F. A., Hirschmann, M. M. & Humayun, M. (2011). The composition of the incipient partial melt of garnet peridotite at 3 GPa and the origin of OIB. *Earth and Planetary Science Letters* **308**, 380–390.

Defant, M. J. & Drummond, M. S. (1990). Derivation of some modern arc magmas by melting of young subducted lithosphere. *Nature* **347**, 662–665.

Donovan, J. J. (2012). *Probe for EPMA: Acquisition, Automation and Analysis, Enterprise Edition*. Probe Software.

Falloon, T. J. & Danyushevsky, L. V. (2000). Melting of refractory mantle at 1·5, 2 and 2·5 GPa under anhydrous and H_2O-undersaturated conditions: implications for the petrogenesis of high-Ca boninites and the influence of subduction components on mantle melting. *Journal of Petrology* **41**, 257–283.

Falloon, T. J., Green, D. H., Danyushevsky, L. V. & Faul, U. H. (1999). Peridotite melting at 1·0 and 1·5 GPa: an experimental evaluation of techniques using diamond aggregates and mineral mixes for determining near-solidus melts. *Journal of Petrology* **40**, 1343–1375.

Falloon, T. J., Green, D. H., Danyushevsky, L. V. & McNeill, A. W. (2008). The composition of near-solidus partial melts of fertile peridotite at 1 and 1·5 GPa: implications for the petrogenesis of MORB. *Journal of Petrology* **49**, 591–613.

Feig, S. T., Koepke, J. & Snow, J. (2006). Effect of water on tholeiitic basalt phase equilibria: an experimental study under

oxidizing conditions. *Contributions to Mineralogy and Petrology* **152**, 611–638.
Ford, C. E., Russell, D. G., Craven, J. A. & Fist, M. R. (1983). Olivine–liquid equilibria: temperature, pressure and composition dependence of the crystal/liquid cation partition coefficients for Mg, Fe^{2+}, Ca and Mn. *Journal of Petrology* **24**, 256–265.
Fyfe, W. S. & McBirney, A. R. (1975). Subduction and the structure of andesitic volcanic belts. *American Journal of Science* **275-A**, 285–297.
Gaetani, G. A. & Grove, T. L. (1998). The influence of water on melting of mantle peridotite. *Contributions to Mineralogy and Petrology* **131**, 323–346.
Gaetani, G. A., O'Leary, J. A., Shimizu, N., Bucholz, C. E. & Newville, M. (2012). Rapid reequilibration of H_2O and oxygen fugacity in olivine-hosted melt inclusions. *Geology* **40**, 915–918.
Gavrilenko, M., Ozerov, A., Kyle, P. R., Carr, M. J., Nikulin, A., Vidito, C. & Danyushevsky, L. (2016). Abrupt transition from fractional crystallization to magma mixing at Gorely volcano (Kamchatka) after caldera collapse. *Bulletin of Volcanology* **78**, 1–28.
Gazel, E., Carr, M. J., Hoernle, K., Feigenson, M. D., Szymanski, D., Hauff, F. & van den Bogaard, P. (2009). Galapagos-OIB signature in southern Central America: Mantle refertilization by arc–hot spot interaction. *Geochemistry, Geophysics, Geosystems* **10**, Q02S11.
Gazel, E., Hoernle, K., Carr, M. J., Herzberg, C., Saginor, I., van den Bogaard, P., Hauff, F., Feigenson, M. & Swisher, C., III (2011). Plume–subduction interaction in southern Central America: Mantle upwelling and slab melting. *Lithos* **121**(**1–4**), 117–134.
Ghiorso, M. S. & Sack, R. O. (1995). Chemical mass transfer in magmatic processes IV. A revised and internally consistent thermodynamic model for the interpolation and extrapolation of liquid–solid equilibria in magmatic systems at elevated temperatures and pressures. *Contributions to Mineralogy and Petrology* **119**, 197–212.
Gill, J. B. (1981). *Orogenic Andesites and Plate Tectonics*. Springer, 390 pp.
Gorbach, N., Portnyagin, M. & Tembrel, I. (2013). Volcanic structure and composition of Old Shiveluch volcano, Kamchatka. *Journal of Volcanology and Geothermal Research* **263**, 193–208.
Gorbach, N. V. & Portnyagin, M. V. (2011). Geology and petrology of the lava complex of Young Shiveluch Volcano, Kamchatka. *Petrology* **19**, 134–166.
Grove, T. L., Kinzler, R. J. & Bryan, W. B. (1992). Fractionation of mid-ocean ridge basalt (MORB). Mantle flow and melt generation at mid-ocean ridges. In: Phipps Morgan, J., Blackman, D. K. & Sinton, J. M. (eds)*Mantle Flow and Melt Generation at Mid-Ocean Ridges. American Geophysical Union, Geophysical Monograph* **71**, 281–310.
Grove, T. L., Chatterjee, N., Parman, S. W. & Medard, E. (2006). The influence of H_2O on mantle wedge melting. *Earth and Planetary Science Letters* **249**, 74–89.
Hauri, E. H. (2002). SIMS analysis of volatiles in silicate glasses, 2: isotopes and abundances in Hawaiian melt inclusions. *Chemical Geology* **183**, 115–141.
Hauri, E. H., Gaetani, G. A. & Green, T. H. (2006). Partitioning of water during melting of the Earth's upper mantle at H_2O-undersaturated conditions. *Earth and Planetary Science Letters* **248**, 715–734.
Hays, M. R. (2004). Intra-transform volcanism along the Siqueiros Fracture Zone 8°20′–8°30′N, East Pacific Rise. M.Sc. thesis, Gainesville, FL: University of Florida.
Herzberg, C. (2006). Petrology and thermal structure of the Hawaiian plume from Mauna Kea volcano. *Nature* **444**, 605–609.
Herzberg, C. (2011). Identification of source lithology in the Hawaiian and Canary Islands: implications for origins. *Journal of Petrology* **52**, 113–146.
Herzberg, C. & Asimow, P. D. (2015). PRIMELT3 MEGA.XLSM software for primary magma calculation: peridotite primary magma MgO contents from the liquidus to the solidus. *Geochemistry, Geophysics, Geosystems* **16**, 563–578.
Herzberg, C. & Gazel, E. (2009). Petrological evidence for secular cooling in mantle plumes. *Nature* **458**, 619–622.
Herzberg, C. & O'Hara, M. J. (2002). Plume-associated ultramafic magmas of Phanerozoic age. *Journal of Petrology* **43**, 1857–1883.
Herzberg, C. & Zhang, J. (1996). Melting experiments on anhydrous peridotite KLB-1: Compositions of magmas in the upper mantle and transition zone. *Journal of Geophysical Research* **101**, 8271–8295.
Herzberg, C., Asimow, P. D., Arndt, N., Niu, Y., Lesher, C. M., Fitton, J. G., Cheadle, M. J. & Saunders, A. D. (2007). Temperatures in ambient mantle and plumes: constraints from basalts, picrites and komatiites. *Geochemistry, Geophysics, Geosystems* **8**, doi:10.1029GC001390.
Herzberg, C., Asimow, P., Ionov, D., Vidito, C., Jackson, M. G. & Geist, D. (2013). Nickel and helium evidence for melt above the core–mantle boundary. *Nature* **493**, 393–397.
Hirose, K. & Kawamoto, T. (1995). Hydrous partial melting of lherzolite at 1 GPa: the effect of H_2O on the genesis of basaltic magmas. *Earth and Planetary Science Letters* **133**, 463–473.
Ionov, D. A. (2010). Petrology of mantle wedge lithosphere: new data on supra-subduction zone peridotite xenoliths from the andesitic Avacha volcano, Kamchatka. *Journal of Petrology* **51**, 327–361.
Iwasaki, T., Levin, V., Nikulin, A. & Iidaka, T. (2013). Constraints on the Moho in Japan and Kamchatka. *Tectonophysics* **609**, 184–201.
Jurewicz, A. J. G. & Watson, E. B. (1988). Cations in olivine, Part 1: Calcium partitioning and calcium–magnesium distribution between olivines and coexisting melts, with petrological applications. *Contributions to Mineralogy and Petrology* **99**, 176–185.
Kamenetsky, V. S., Elburg, M., Arculus, R. & Thomas, R. (2006). Magmatic origin of low-Ca olivine in subduction-related magmas: co-existence of contrasting magmas. *Chemical Geology* **233**, 346–357.
Kamenetsky, V. S., Pompilio, M., Métrich, N., Sobolev, A. V., Kuzmin, D. V. & Thomas, R. (2007). Arrival of extremely volatile-rich high-Mg magmas changes explosivity of Mount Etna. *Geology* **35**, 255–258.
Kayzar, T. M., Nelson, B. K., Bachmann, O., Bauer, A. M. & Izbekov, P. E. (2014). Deciphering petrogenic processes using Pb isotope ratios from time-series samples at Bezymianny and Klyuchevskoy volcanoes, Central Kamchatka Depression. *Contributions to Mineralogy and Petrology* **168**, 1–28.
Kelemen, P. B., Shimizu, N. & Salters, V. J. M. (1995). Extraction of mid-ocean ridge basalt from the upwelling mantle by focused flow of melt in dunite channels. *Nature* **375**, 747–753.
Kelemen, P. B., Hirth, G., Shimizu, N., Spiegelman, M. & Dick, H. J. B. (1997). A review of melt migration processes in the adiabatically upwelling mantle beneath oceanic spreading centers. *Philosophical Transactions of the Royal Society of London, Series A* **355**, 283–318.
Kelemen, P. B., Hart, S. R. & Bernstein, S. (1998). Silica enrichment in the continental upper mantle via melt/rock reaction. *Earth and Planetary Science Letters* **164**, 387–406.

Kelemen, P. B., Yogodzinski, G. M. & Scholl, D. W. (2003). Along-strike variation in the Aleutian island arc: Genesis of high Mg# andesite and implications for continental crust. In: Eiler, J. M. (ed.) *Inside the Subduction Factory. American Geophysical Union, Geophysical Monograph* **138**, 223–276.

Kelley, K., Plank, T., Newman, S., Stolper, E., Grove, T., Parman, S. & Hauri, E. (2010). Mantle melting as a function of water content beneath the Mariana Arc. *Journal of Petrology* **51**, 1711–1738.

Kessel, R., Schmidt, M. W., Ulmer, P. & Pettke, T. (2005). Trace element signature of subduction-zone fluids, melts and supercritical liquids at 120–180 km depth. *Nature* **437**, 724–727.

Kinzler, R. J. (1997). Melting of mantle peridotite at pressures approaching the spinel to garnet transition: Application to mid-ocean ridge basalt petrogenesis. *Journal of Geophysical Research* **102**, 853–874.

Kinzler, R. J. & Grove, T. L. (1992). Primary magmas of mid-ocean ridge basalts, 1. Experiments and methods. *Journal of Geophysical Research* **97**, 6885–6906.

Koga, K. T., Kelemen, P. B. & Shimizu, N. (2001). Petrogenesis of the crust–mantle transition zone and origin of lower crustal wehrlite in the Oman ophiolite. *Geochemistry, Geophysics, Geosystems* **2**, 200GC000132.

Laporte, D., Toplis, M. J., Seyler, M. & Devidal, J.-L. (2004). A new experimental technique for extracting liquids from peridotite at very low degrees of melting: application to partial melting of depleted peridotite. *Contributions to Mineralogy and Petrology* **146**, 463–484.

Lees, J. M., Symons, N., Chubarova, O., Gorelchik, V. & Ozerov, A. (2007). Tomographic images of Klyuchevskoy Volcano P-wave velocity. In: Eichelberger, J., Gordeev, E., Izbekov, P., Kasahara, M. & Lees, J. (eds) *Volcanism and Subduction: The Kamchatka Region. American Geophysical Union, Geophysical Monograph* **172**, 293–302.

Le Roux, V., Dasgupta, R. & Lee, C.-T. A. (2011). Mineralogical heterogeneities in the Earth's mantle: constraints from Mn, Co, Ni and Zn partitioning during partial melting. *Earth and Planetary Science Letters* **307**, 395–408.

Levin, V., Shapiro, N., Park, J. & Ritzwoller, M. (2002). Seismic evidence for catastrophic slab loss beneath Kamchatka. *Nature* **418**, 763–767.

Levin, V., Droznina, S., Gavrilenko, M., Carr, M. J. & Senyukov, S. (2014). Seismically active subcrustal magma source of the Klyuchevskoy volcano in Kamchatka, Russia. *Geology* **42**, 983–986.

Le Voyer, M., Asimow, P. D., Mosenfelder, J. D., Guan, Y., Wallace, P. J., Schiano, P., Stolper, E. M. & Eiler, J. M. (2014). Zonation of H_2O and F concentrations around melt inclusions in olivines. *Journal of Petrology* **55**, 685–707.

Li, C., Ripley, E. M., Thakurta, J., Stifter, E. C. & Qi, L. (2013). Variations of olivine Fo–Ni contents and highly chalcophile element abundances in arc ultramafic cumulates, southern Alaska. *Chemical Geology* **351**, 15–28.

Libourel, G. (1999). Systematics of calcium partitioning between olivine and silicate melt: implications for melt structure and calcium content of magmatic olivines. *Contributions to Mineralogy and Petrology* **136**, 63–80.

Lloyd, A., Plank, T., Ruprecht, P., Hauri, E. & Rose, W. (2013). Volatile loss from melt inclusions in pyroclasts of differing sizes. *Contributions to Mineralogy and Petrology* **165**, 129–153.

Longhi, J., Durand, S. & Walker, D. (2010). The pattern of Ni and Co abundances in lunar olivines. *Geochimica et Cosmochimica Acta* **74**, 784–798.

Manning, C. E. (2004). The chemistry of subduction-zone fluids. *Earth and Planetary Science Letters* **223**, 1–16.

Matzen, A. K., Baker, M. B., Beckett, J. R. & Stolper, E. M. (2011). Fe–Mg partitioning between olivine and high-magnesian melts and the nature of Hawaiian parental liquids. *Journal of Petrology* **52**, 1243–1263.

Matzen, A. K., Baker, M. B., Beckett, J. R. & Stolper, E. M. (2013). The temperature and pressure dependence of nickel partitioning between olivine and silicate melt. *Journal of Petrology* **54**, 2521–2545.

Melekescev, I. V. (1980). *Volcanism and Relief-Formation*. Nauka, 212 pp. (in Russian).

Mibe, K., Fujii, T., Yasuda, A. & Ono, S. (2006). Mg–Fe partitioning between olivine and ultramafic melts at high pressures. *Geochimica et Cosmochimica Acta* **70**, 757–766.

Mironov, N., Portnyagin, M., Botcharnikov, R., Gurenko, A., Hoernle, K. & Holtz, F. (2015). Quantification of the CO_2 budget and H_2O–CO_2 systematics in subduction-zone magmas through the experimental hydration of melt inclusions in olivine at high H_2O pressure. *Earth and Planetary Science Letters* **425**, 1–11.

Mironov, N. L. & Portnyagin, M. V. (2011). H_2O and CO_2 in parental magmas of Kliuchevskoi volcano inferred from study of melt and fluid inclusions in olivine. *Russian Geology and Geophysics* **52**, 1353–1367.

Müntener, O., Kelemen, P. B. & Grove, T. L. (2001). The role of H_2O during crystallization of primitive arc magmas under uppermost mantle conditions and genesis of igneous pyroxenites: an experimental study. *Contributions to Mineralogy and Petrology* **141**, 643–658.

Mysen, B. (2007). Partitioning of calcium, magnesium, and transition metals between olivine and melt governed by the structure of the silicate melt at ambient pressure. *American Mineralogist* **92**, 844–862.

Mysen, B. O. (2008). Olivine/melt transition metal partitioning, melt composition, and melt structure—melt polymerization and *Qn*-speciation in alkaline earth silicate systems. *Geochimica et Cosmochimica Acta* **72**, 4796–4812.

Nandedkar, R. H., Ulmer, P. & Müntener, O. (2014). Fractional crystallization of primitive, hydrous arc magmas: an experimental study at 0·7 GPa. *Contributions to Mineralogy and Petrology* **167**, 1015.

Newcombe, M. E., Fabbrizio, A., Zhang, Y., Ma, C., Le Voyer, M., Guan,Y., Eiler, J. M., Saal, A. E. & Stolper, E. M. (2014). Chemical zonation in olivine-hosted melt inclusions. *Contributions to Mineralogy and Petrology* **168**, 1030.

Nikulin, A., Levin, V., Carr, M., Herzberg, C. & West, M. (2012). Evidence for two upper mantle sources driving volcanism in Central Kamchatka. *Earth and Planetary Science Letters* **321–322**, 14–19.

Ozerov, A. Y. (2000). The evolution of high-alumina basalts of the Klyuchevskoy volcano, Kamchatka, Russia, based on microprobe analyses of mineral inclusions. *Journal of Volcanology and Geothermal Research* **95**, 65–79.

Ozerov, A. Y. (2009). Experimental modeling of the explosion mechanism of basaltic magmas. *Petrology* **17**, 653–668.

Ozerov, A. Y., Ariskin, A. A., Kyle, P., Bogoyavlenskaya, G. E. & Karpenko, S. F. (1997). Petrological–geochemical model for genetic relationships between basaltic and andesitic magmatism of Klyuchevskoi and Bezymyannyi volcanoes, Kamchatka. *Petrology* **5**, 550–569.

Parman, S. & Grove, T. L. (2004). Harzburgite melting with and without H_2O: experimental data and predictive modeling. *Journal of Geophysical Research* **109**, doi:10.1029/2003JB002566.

Parman, S. W., Dann, J. C., Grove, T. L. & deWit, M. J. (1997). Emplacement conditions of komatiite magmas from the 3·49 Ga Komati Formation, Barberton Greenstone Belt,

South Africa. *Earth and Planetary Science Letters* **150**, 303–323.

Perfit, M. R., Fornari, D. J., Ridley, W. I., Kirk, P. D., Casey, J., Kastens, K. A., Reynolds, J. R., Edwards, M., Desonie, D., Shuster, R. & Paradis, S. (1996). Recent volcanism in the Siqueiros transform fault: picritic basalts and implications for MORB magma genesis. *Earth and Planetary Science Letters* **141**, 91–108.

Plank, T., Kelley, K. A., Zimmer, M. M., Hauri, E. H. & Wallace, P. J. (2013). Why do mafic arc magmas contain ~4 wt % water on average? *Earth and Planetary Science Letters* **364**, 168–179.

Ponomareva, V. V., Kyle, P., Pevzner, M. M., Sulerzhitsky, L. D. & Hartman, M. (2007). Holocene eruptive history of Shiveluch Volcano, Kamchatka Peninsula, Russia. In: Eichelberger, J., Gordeev, E., Izbekov, P., Kasahara, M. & Lees, J. (eds) *Volcanism and Subduction: The Kamchatka Region. American Geophysical Union, Geophysical Monograph* **172**, 263–282.

Portnyagin, M., Hoernle, K., Avdeiko, G., Hauff, F., Werner, R., Bindeman, I., Uspensky, V. & Garbe-Schonberg, D. (2005). Transition from arc to oceanic magmatism at the Kamchatka–Aleutian junction. *Geology* **33**, 25–28.

Portnyagin, M., Bindeman, I. N., Hoernle, K. & Hauff, F. (2007a). Geochemistry of primitive lavas of the Central Kamchatka depression: magma generation at the edge of the Pacific Plate. In: Eichelberger, J., Gordeev, E., Izbekov, P., Kasahara, M. & Lees, J. (eds) *Volcanism and Subduction: The Kamchatka Region. American Geophysical Union, Geophysical Monograph* **172**, 199–239.

Portnyagin, M., Hoernle, K., Plechov, P., Mironov, N. & Khubunaya, S. (2007b). Constraints on mantle melting and composition and nature of slab components in volcanic arcs from volatiles (H_2O, S, Cl, F) and trace elements in melt inclusions from Kamchatka Arc. *Earth and Planetary Science Letters* **255**, 53–69.

Portnyagin, M., Almeev, R., Matveev, S. & Holtz, F. (2008). Experimental evidence for rapid water exchange between melt inclusions in olivine and host magma. *Earth and Planetary Science Letters* **272**, 541–552.

Portnyagin, M., Hoernle, K. & Mironov, N. L. (2014). Contrasting compositional trends of rocks and olivine-hosted melt inclusions from Cerro Negro volcano (Central America): implications for decompression-driven fractionation of hydrous magmas. *International Journal of Earth Sciences* **103**, 1963–1982.

Qian, Q., O'Neill, H. St. C. & Hermann, J. (2010). Comparative diffusion coefficients of major and trace elements in olivine at ~950 °C from a xenocryst included in dioritic magma. *Geology* **38**, 331–334.

Roberge, J., Wallace, P. J., White, R. V. & Coffin, M. F. (2005). Anomalous uplift and subsidence of the Ontong Java Plateau inferred from CO_2 contents of submarine basaltic glasses. *Geology* **33**, 501–504.

Robinson, J. A. C., Wood, B. J. & Blundy, J. D. (1998). The beginning of melting of fertile and depleted peridotite at 1·5 GPa. *Earth and Planetary Science Letters* **155**, 97–111.

Roggensack, K. (2001). Sizing up crystals and their melt inclusions: a new approach to crystallization studies. *Earth and Planetary Science Letters* **187**, 221–237.

Roggensack, K., Hervig, R. L., McKnight, S. B. & Williams, S. N. (1997). Explosive basaltic volcanism from Cerro Negro volcano: influence of volatiles on eruptive style. *Science* **277**, 1639–1642.

Ruprecht, P. & Plank, T. (2013). Feeding andesitic eruptions with a high-speed connection from the mantle. *Nature* **500**, 68–72.

Saal, A. E., Hauri, E. H., Langmuir, C. H. & Perfit, M. R. (2002). Vapour undersaturation in primitive mid-ocean-ridge basalt and the volatile content of Earth's upper mantle. *Nature* **419**, 451–455.

Sadofsky, S. J., Portnyagin, M., Hoernle, K. & van den Bogaard, P. (2008). Subduction cycling of volatiles and trace elements through the Central American volcanic arc: evidence from melt inclusions. *Contributions to Mineralogy and Petrology* **155**, 433–456.

Sano, T. & Yamashita, S. (2004). Experimental petrology of basement lavas from Ocean Drilling Program Leg 192: implications for differentiation processes in Ontong Java Plateau magmas. In: Fitton, J. G., Mahoney, J. J., Wallace, P. J. & Saunders, A. D. (eds) *Origin and Evolution of the Ontong Java Plateau. Geological Society, London, Special Publications* **229**, 185–218.

Seligman, A., Bindeman, I., Jicha, B., Ellis, B., Ponomareva, V. & Leonov, V. (2014). Multi-cyclic and isotopically diverse silicic magma generation in an arc volcano: Gorely eruptive center, Kamchatka, Russia. *Journal of Petrology* **55**, 1561–1594.

Shaw, A. M., Hauri, E. H., Fischer, T. P., Hilton, D. R. & Kelley, K. A. (2008). Hydrogen isotopes in Mariana arc melt inclusions: implications for subduction dehydration and the deep-Earth water cycle. *Earth and Planetary Science Letters* **275**, 138–145.

Sobolev, A. V., Hofmann, A. W., Sobolev, S. V. & Nikogosian, I. K. (2005). An olivine-free mantle source of Hawaiian shield basalts. *Nature* **434**, 590–597.

Sobolev, A. V., Hofmann, A. W., Kuzmin, D. V., Yaxley, G. M., Arndt, N. T., Chung, S.-L., Danyushevsky, L. V., Elliott, T., Frey, F. A., Garcia, M. O., Gurenko, A. A., Kamenetsky, V. S., Kerr, A. C., Krivolutskaya, N. A., Matvienkov, V. V., Nikogosian, I. K., Rocholl, A., Sigurdsson, I. A., Sushchevskaya, N. M. & Teklay, M. (2007). The amount of recycled crust in sources of mantle-derived melts. *Science* **316**, 412–417.

Sobolev, A. V., Krivolutskaya, N. A. & Kuzmin, D. V. (2009a). Petrology and parental melts and mantle sources of Siberian Trap magmatism. *Petrology* **17**, 253–286.

Sobolev, A. V., Sobolev, S. V., Kuzmin, D. V., Malitch, K. N. & Petrunin, A. G. (2009b). Siberian meimechites: origin and relation to flood basalts and kimberlites. *Russian Geology and Geophysics* **50**, 999–1033.

Sobolev, A. V., Hofmann, A. W., Jochum, K. P., Kuzmin, D. V. & Stoll, B. (2011). A young source for the Hawaiian plume. *Nature* **476**, 434–437.

Stolper, E. & Newman, S. (1994). The role of water in the petrogenesis of Mariana Trough magmas. *Earth and Planetary Science Letters* **121**, 293–325.

Straub, S. M., LaGatta, A. B., Martin-Del Pozzo, A. L. & Langmuir, C. H. (2008). Evidence from high Ni olivines for a hybridized peridotite/pyroxenite source for orogenic andesites from the central Mexican Volcanic Belt. *Geochemistry, Geophysics, Geosystems* **9**, Q03007.

Straub, S. M., Gómez-Tuena, A., Stuart, F. M., Zellmer, G. F., Espinasa-Perena, R., Cai, M. Y. & Iizuka,Y. (2011). Formation of hybrid arc andesites beneath thick continental crust. *Earth and Planetary Science Letters* **303**, 337–347.

Suhr, G., Hellebrand, E., Snow, J. E., Seck, H. A. & Hofmann, A. W. (2003). Significance of large, refractory dunite bodies in the upper mantle of the Bay of Islands ophiolite. *Geochemistry, Geophysics, Geosystems* **4**, doi:10.1029/2001GC000277.

Takahashi, E. & Kushiro, I. (1983). Melting of a dry peridotite at high pressures and basalt magma genesis. *American Mineralogist* **68**, 859–879.

Taura, H., Yurimoto, H., Kurita, K. & Sueno, S. (1998). Pressure dependence on partition coefficients for trace elements between olivine and the coexisting melts. *Physics and Chemistry of Minerals* **25**, 469–484.

Tenner, T. J., Hirschmann, M. M., Withers, A. C. & Hervig, R. L. (2009). Hydrogen partitioning between nominally anhydrous upper mantle minerals and melt between 3 and 5 GPa and applications to hydrous peridotite partial melting. *Chemical Geology* **262**, 42–56.

Tenner, T. J., Hirschmann, M. M. & Munir, H. (2012). The effect of H_2O on partial melting of garnet peridotite at 3·5 GPa. *Geochemistry, Geophysics, Geosystems* **13**, Q03016.

Till, C. B., Grove, T. L. & Krawczynski, M. J. (2012). A melting model for variably depleted and enriched lherzolite in the plagioclase and spinel stability fields. *Journal of Geophysical Research* **117**, B06206.

Tolstykh, M. L., Naumov, V. B., Gavrilenko, M. G., Ozerov, A. Y. & Kononkova, N. N. (2012). Chemical composition, volatile components, and trace elements in the melts of the Gorely volcanic center, southern Kamchatka: Evidence from inclusions in minerals. *Geochemistry International* **50**, 522–550.

Toplis, M. J. & Carroll, M. R. (1995). An experimental study of the influence of oxygen fugacity on Fe–Ti oxide stability, phase relations, and mineral–melt equilibria in ferro-basaltic systems. *Journal of Petrology* **36**, 1137–1170.

Tuff, J. & O'Neill, H. St. C. (2010). The effect of sulfur on the partitioning of Ni and other first-row transition elements between olivine and silicate melt. *Geochimica et Cosmochimica Acta* **74**, 6180–6205.

Vidito, C., Herzberg, C., Gazel, E., Geist, D. & Harpp, K. (2013). Lithological structure of the Galápagos Plume. *Geochemistry, Geophysics, Geosystems* **14**, doi:10.1002/ggge.20270.

Volynets, O. N., Ponomareva, V. V. & Babansky, A. D. (1997). Magnesian basalts of Shiveluch andesite volcano, Kamchatka. *Petrology* **5**, 183–196.

Wallace, P. J. (2005). Volatiles in subduction zone magmas: concentrations and fluxes based on melt inclusion and volcanic gas data. *Journal of Volcanology and Geothermal Research* **140**, 217–240.

Walter, M. J. (1998). Melting of garnet peridotite and the origin of komatiite and depleted lithosphere. *Journal of Petrology* **39**, 29–60.

Wang, Z. & Gaetani, G. A. (2008). Partitioning of Ni between olivine and siliceous eclogite partial melt: experimental constraints on the mantle source of Hawaiian basalts. *Contributions to Mineralogy and Petrology* **156**, 661–678.

Wasylenki, L. E., Baker, M. B., Kent, A. J. R. & Stolper, E. M. (2003). Near-solidus melting of the shallow upper mantle: Partial melting experiments on depleted peridotite. *Journal of Petrology* **44**, 1163–1191.

Watson, E. B. (1979). Calcium content of forsterite coexisting with silicate liquid in the system Na_2O–CaO–MgO–Al_2O_3–SiO_2. *American Mineralogist* **64**, 824–829.

Wehrmann, H., Hoernle, K., Portnyagin, M., Wiedenbeck, M. & Heydolph, K. (2011). Volcanic CO_2 output at the Central American subduction zone inferred from melt inclusions in olivine crystals from mafic tephras. *Geochemistry, Geophysics, Geosystems* **12**, Q06003.

Yang, H.-J., Kinzler, R. J. & Grove, T. L. (1996). Experiments and models of anhydrous basaltic olivine–plagioclase–augite saturated melts from 0·001 to 10 kbar. *Contributions to Mineralogy and Petrology* **124**, 1–18.

Zimmer, M. M., Plank, T., Hauri, E. H., Yogodzinski, G. M., Stelling, P., Larsen, J., Singer, B., Jicha, B., Mandeville, C. & Nye, C. J. (2010). The role of water in generating the calc-alkaline trend: new volatile data for Aleutian magmas and a new tholeiitic index. *Journal of Petrology* **51**, 2411–2444.